

Article

Spatiotemporal Evolution and Hysteresis Analysis of Drought Based on Rainfed-Irrigated Arable Land

Enyu Du ^{1,2,3} , Fang Chen ^{1,2,3,4,*}, Huicong Jia ^{1,2} , Lei Wang ^{1,2}  and Aqiang Yang ^{1,2} 

¹ Key Laboratory of Digital Earth Science, Aerospace Information Research Institute, Chinese Academy of Sciences, Beijing 100094, China

² International Research Center of Big Data for Sustainable Development Goals, Beijing 100094, China

³ University of Chinese Academy of Sciences, Beijing 100049, China

⁴ State Key Laboratory of Remote Sensing Science, Aerospace Information Research Institute, Chinese Academy of Sciences, Beijing 100094, China

* Correspondence: chenfang_group@radi.ac.cn; Tel.: +86-10-8217-8105

Abstract: Drought poses a serious threat to agricultural production and food security in the context of global climate change. Few studies have explored the response mechanism and lag time of agricultural drought to meteorological drought from the perspective of cultivated land types. This paper analyzes the spatiotemporal evolution patterns and hysteresis relationship of meteorological and agricultural droughts in the middle and lower reaches of the Yangtze River in China. Here, the Moderate Resolution Imaging Spectroradiometer (MODIS) vegetation index products and surface temperature products were selected to calculate the Temperature Vegetation Dryness Index (TVDI) from 2010 to 2015. Furthermore, we obtained the Standardized Precipitation Evapotranspiration Index (SPEI) and the Palmer Drought Severity Index (PDSI) for the same period. Based on these indices, we analyzed the correlation and the hysteresis relationship between agricultural and meteorological drought in rainfed and irrigated arable land. The results showed that, (1) compared with SPEI, the high spatial resolution PDSI data were deemed more suitable for the subsequent accurate and scientific analysis of the relationship between meteorological and agricultural droughts. (2) When meteorological drought occurs, irrigated arable land is the first to experience agricultural drought, and then alleviates when the drought is most severe in rainfed arable land, indicating that irrigated arable land is more sensitive to drought events when exposed to the same degree of drought risk. However, rainfed arable land is actually more susceptible to agricultural drought due to the intervention of irrigation measures. (3) According to the cross-wavelet transform analysis, agricultural droughts significantly lag behind meteorological droughts by about 33 days during the development process of drought events. (4) The spatial distribution of the correlation coefficient between the PDSI and TVDI shows that the area with negative correlations of rainfed croplands and the area with positive correlations of irrigated croplands account for 77.55% and 68.04% of cropland areas, respectively. This study clarifies and distinguishes the details of the meteorological-to-agricultural drought relationship in rainfed and irrigated arable land, noting that an accurate lag time can provide useful guidance for drought monitoring management and irrigation project planning in the middle and lower reaches of the Yangtze River.

Keywords: TVDI; PDSI; drought; meteorological drought; spatiotemporal evolution; lag



Citation: Du, E.; Chen, F.; Jia, H.; Wang, L.; Yang, A. Spatiotemporal Evolution and Hysteresis Analysis of Drought Based on Rainfed-Irrigated Arable Land. *Remote Sens.* **2023**, *15*, 1689. <https://doi.org/10.3390/rs15061689>

Academic Editor: Gabriel Senay

Received: 7 January 2023

Revised: 17 March 2023

Accepted: 18 March 2023

Published: 21 March 2023



Copyright: © 2023 by the authors. Licensee MDPI, Basel, Switzerland. This article is an open access article distributed under the terms and conditions of the Creative Commons Attribution (CC BY) license (<https://creativecommons.org/licenses/by/4.0/>).

1. Introduction

Drought is a phenomenon that occurs when a region breaks the balance of precipitation and evapotranspiration over a long period, resulting in the loss of soil moisture and crops or the reduction of surface runoff [1]. The frequency and intensity of droughts show an increasing trend due to the long duration and wide range of influence [2–4]. Drought has caused immeasurable effects on the ecological environment and agricultural production, thus seriously restricting the sustainable development of society [5–8]. A drought is

generally defined by the international meteorological community as a “prolonged precipitation deficit or significant precipitation shortage” and can be divided into four categories: meteorological drought, agricultural drought, hydrological drought, and socioeconomic drought, according to the impact type and scope [9–13]. These four types of droughts are interrelated, and the meteorological drought, as the source and basis of the other three droughts, refers to the unbalanced state of water gain and loss caused by the mismatch between evaporation and precipitation [12–17]. Agricultural drought is a condition that the soil water content cannot meet the needs of plant growth, resulting in a plant water shortage [18]. Although the mechanisms of meteorological and agricultural droughts are different, they have a certain response relationship between them [12–14,16,19]. Therefore, various types of drought monitoring methods and indices have been proposed to describe the changing characteristics or degree of drought development quantitatively.

Meteorological drought monitoring and remote sensing drought monitoring are two common methods of drought monitoring [20–26]. Traditional meteorological drought monitoring usually selects suitable drought indicators to determine the time and extent of droughts based on the data obtained from meteorological stations, agricultural stations, hydrological stations, and other stations, such as the standardized precipitation index (SPI) [27,28], the precipitation anomaly percentage (Pa) [29], the standardized precipitation evapotranspiration index (SPEI) [30], the precipitation Z-index [28], and the Palmer drought severity index (PDSI) [31–33]. However, the occurrence and spatiotemporal characteristics of drought are complex, and when coupled with scattered ground stations and poor representative observation data, it makes it difficult to monitor large-scale droughts quickly and accurately [34–37]. Among them, due to the clear physical meaning and the comprehensive consideration of precipitation and temperature, PDSI is especially suitable for monitoring meteorological drought on a longer time scale and has been widely used in China [38–41].

In addition, as a significant parameter for early drought prediction and monitoring, the drought index can qualitatively determine the development process of drought over a certain period. Therefore, remote sensing technology can be used to calculate ground object parameters such as soil moisture, land surface temperature, crop growth status, and vegetation coverage ratio [42,43]. By establishing a remote sensing drought index model, we can evaluate and monitor the evolution of drought on large spatiotemporal scales [44,45]. Common remote sensing drought indices include the Normalized Difference Vegetation Index (NDVI) [46], Enhanced Vegetation Index (EVI) [47], Vegetation Health Index (VHI) [48,49], Temperature Vegetation Drought Index (TVDI) [50], (Modified) Perpendicular Drought Index (MPDI/PDI) [51–55], Temperature Condition Index (TCI) [56], Drought Severity Index (SDI) [57], Crop Water Stress Index (CWSI) [58], Water Deficit Index (WDI) [59], Surface Water Supply Index (SWSI) [60–62], the Vegetation Supply Water Index (VSWI) [63], etc. Each index has a different focus. Most researchers have shown that the combination of NDVI and Land Surface Temperature (LST) can reveal information about drought conditions. Due to the accurate estimation of surface soil moisture, the TVDI has become one of the most important parameters for remote sensing agricultural drought monitoring [36,64–67]. For example, Shashikant et al. [68] calculated the TVDI based on Landsat 8 and classified the severity of agricultural drought in Malaysia. In order to improve the accuracy of soil moisture inversion by the TVDI, Wang et al. [69] assessed the effects of the TVDI calculated by different vegetation indices in drought monitoring in Northeast China.

Agricultural drought is affected by meteorological drought directly, which occurs later than meteorological drought, and there is usually a hysteresis relationship between them. Assessing meteorological drought is simply based on the available global precipitation data and climatic parameters. However, the development of agricultural drought is relatively complex, and causes serious agricultural economic losses every year, threatening food security and sustainable agricultural development. There may be uncertainties between meteorology and agricultural droughts due to various meteorological or climate factors, such as different climate regions, drought indices, or climate models. Seidenfaden et al. [70]

estimated and compared several drought indices, and explored the linkage between the drought and changing climate to evaluate the potential impact of uncertainties from climate model choices on the indices. Kuśmierk-Tomaszewska et al. [71] found the relationship between meteorological and agricultural drought indicators is significant, which can allow for the determination of crop water deficits from the indicators to guide irrigation needs in the study area. Behrang Manesh et al. [72] investigated the relationship between meteorological and agricultural droughts in different climates of Iran during the growing season based on the correlation analysis between SPEI and VHI. Furthermore, global scholars have conducted extensive research exploring the response of agricultural drought to meteorological drought [73,74]. Tian et al. [75] constructed the Comprehensive Agricultural Drought Index (CADI) based on the hysteresis effect of soil moisture on meteorological factors and compared it with various other indices to evaluate and verify the degree of drought. Hu et al. [76] calculated the time-lag relationships among meteorological, agricultural, and hydrological droughts using the grey relational analysis method and the SWAT model. However, most research has focused on the formation and spread of drought in the whole region. For example, Li et al. [77] only calculated the propagation time of meteorological droughts to agricultural droughts in typical rain-fed agricultural areas of the Loess Plateau in China but ignored irrigated arable land. Alahacoon et al. [78] also only monitored long-term drought in the entire region of Sri Lanka to assess the impact on the country's economy. Few researches have explored the response mechanism and hysteresis relationship of agricultural drought to meteorological drought based on arable land types and compared the differences between rainfed and irrigated arable land [16,79]. In the context of the increasing global warming; therefore, studying the evolution discipline, formation, and transmission mechanism of meteorological drought to agricultural drought have important reference value for promoting the development of the regional economy. In addition, this study distinguishes between rainfed and irrigated cultivated land, which can provide new ideas and directions for related drought researchers.

Agricultural production occupies an important position in the development of the national economy. The middle and lower reaches of the Yangtze River, one of the most significant grain-producing areas in China [80–83], are threatened by drought frequently due to the extreme climate, irrigation, and topography in recent years [82]. In particular, about 56.96 million people and 58,120 square kilometers of crops were affected by the extreme drought events due to the high temperatures and the abnormally low precipitation in the summer of 2013, with a direct economic loss of CNY 36.64 billion [82]. Therefore, investigating the transmission mechanism and lag time between meteorological and agricultural droughts can provide an alternative method for studying the evolutionary characteristics of agricultural drought.

This study mainly analyzes the temporal and spatial evolution pattern and hysteresis relationship between meteorological drought and agricultural drought. The key research objectives are as follows: (1) identify the drought events and analyze the applicability and feasibility of the PDSI in monitoring meteorological drought, (2) analyze the potential of the PDSI and TVDI to monitor meteorological and agricultural droughts in the middle and lower reaches of the Yangtze River, (3) describe the impact degree of meteorological droughts to agricultural droughts in rainfed and irrigated land, respectively, and (4) analyze the lag relationship of rainfed and irrigated land between meteorological droughts and agricultural droughts according to the cross-wavelet transform and Pearson's correlation analysis method. This study focuses on different types of arable land, which has a certain reference value for promoting economic development in the middle and lower reaches of the Yangtze River.

2. Materials and Methods

2.1. Study Area

The middle and lower reaches of the Yangtze River occupy the area north of the Nanling, south of the Qinling mountains–HuaiHe River line, and east of the Wu Mountains

(105°E–123°E, 25°–34°N). The region is in the subtropical monsoon climate zone, with an altitude of 5–100 m, flat terrain, and plenty of rivers and lakes. It has sufficient precipitation, about 1000–1400 mm per year, though it is unevenly distributed, resulting in frequent droughts and floods [84]. The annual average temperature of the area is 14–18 °C. As one of the three major plains in China, the middle and lower reaches of the Yangtze River is a significant grain base and a production base for important economic crops such as oil, hemp, and cotton, making it a major agricultural area and the most economically developed zone in China [80–83,85].

Based on the two high temperature and severe drought events in southern China during the spring and summer of 2011 and 2013 summer, the important provinces involved in the disaster were selected, including Chongqing, Guizhou, Hubei, Hunan, Anhui, Jiangxi, and Zhejiang. According to the United States Geological Survey's 1-km Global Food Security Support Analysis Data (GFSAD) [86–89], Northern Anhui, Northern Hubei, Central Chongqing, Western Guizhou, and the southeastern coastal areas of Zhejiang are primarily irrigated agriculture, while Hunan, Jiangxi, and Southern Hubei are dominated by rainfed agriculture. The geographical location, elevation, and distribution of agricultural land categories in the study area are illustrated in Figure 1.

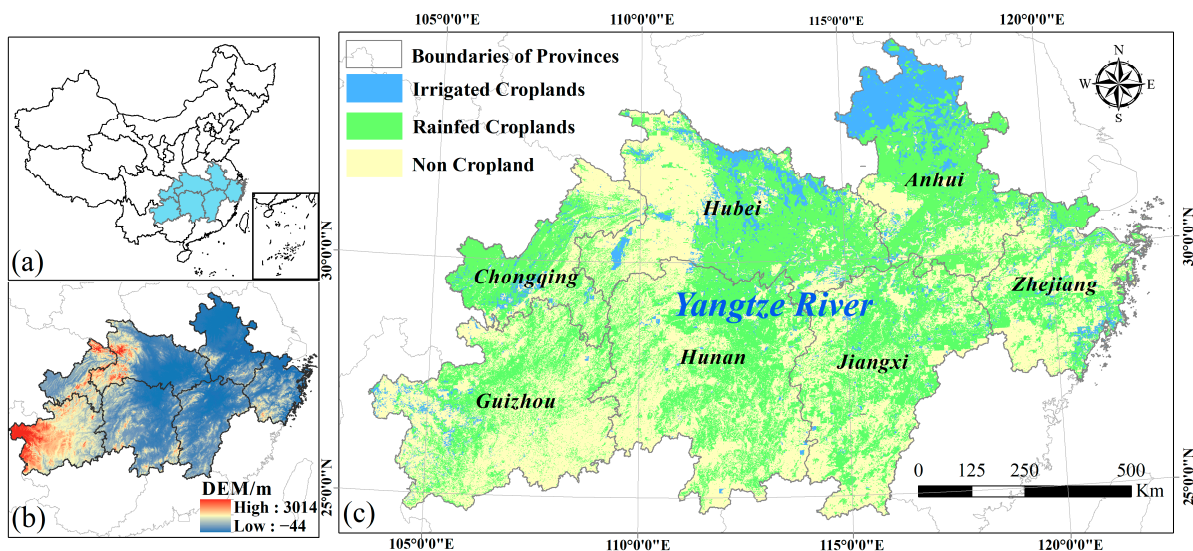


Figure 1. The cropland types and elevation of the middle and lower reaches of the Yangtze River in China. (a) Location of the study area in China. (b) Digital elevation model map of the study area. (c) Irrigated and rainfed croplands map of the study area.

2.2. Data

The remote sensing data selected is the Moderate-resolution Imaging Spectroradiometer (MODIS) satellite data in this paper, sourced from the National Aeronautics and Space Administration (NASA), including the NDVI product MOD13Q1 and the land surface temperature (LST) product MOD11A2, with the spatial resolutions of 250 m × 250 m and 1 km × 1 km, respectively. The meteorological drought index selected and compared in this article are the Standardized Precipitation-Evapotranspiration Index (SPEI) [30,90,91] and the Palmer Drought Severity Index (PDSI) [31–33], which are respectively derived from the global SPEI database and the TerraClimate database [92]. The SPEI database provides long-term and reliable information about global drought conditions with a 0.5-degree spatial resolution and a monthly temporal resolution. It can provide SPEI data on different timescales from 1 to 48 months. The PDSI estimates soil moisture supply and demand based on precipitation and temperature and is used to study the temporal and spatial characteristics of drought to monitor large-scale droughts. Both SPEI and PDSI are widely used in meteorological drought monitoring. SPEI with multi-scale features can help us demonstrate the accuracy of drought events. However, the lower spatial resolution of

SPEI data (50 km) may lead to large uncertainties for further analysis. For the middle and lower reaches of the Yangtze River in China, the PDSI is mainly chosen for subsequent research and analysis due to its higher spatial resolution. Other auxiliary data include basic geographic data, such as administrative divisions and digital elevation models. According to the drought events that occurred in 2011 and 2013 recorded in the historical disaster database of the National Disaster Reduction Center of the Ministry of Emergency Management, the data from 2010 to 2015 were selected.

Using the Google Earth Engine (GEE) platform and the study area vector files, the MOD11A2 and MOD13Q1 data for the whole year of 2010–2015 were obtained. The MOD11A2 data were resampled to a 250 m spatial resolution before downloading based on GEE. To monitor and determine the accuracy of drought events, this study downloaded the SPEI data on four different time scales and analyzed the sensitivity of the SPEI data on different timescales to drought events. High spatial resolution PDSI data were downloaded as the main meteorological drought index data in this research. All PDSI data were resampled from 4 km to 250 m spatial resolution by using the “Nearest” method in the *Resample* module based on ArcGIS 10.8 software. The Global Food Security Support Analysis Data Crop Mask Global 1-km dataset (GFSAD1KCM), which can distinguish between rainfed croplands and irrigated croplands, was superimposed to investigate the comprehensive response of different agricultural regions to meteorological and agricultural droughts. Details of the remote sensing data and auxiliary data are shown in Table 1.

Table 1. Details of the remote sensing datasets and auxiliary datasets.

Data Set	Coverage	Period	Frequency	Resolution
MOD13Q1	Global	2010–2015	16-daily	250 m × 250 m
MOD11A2	Global	2010–2015	8-daily	1 km × 1 km
SPEI	Global	2010–2015	Monthly	0.5° × 0.5°
PDSI	Global	2010–2015	Monthly	4 km × 4 km
GFSAD1KCM	Cropland extent	2010	/	1 km × 1 km
DEM	Global	/	/	30 m × 30 m

2.3. Methods

2.3.1. Standardized Precipitation Evapotranspiration Index (SPEI) and Palmer Drought Severity Index (PDSI)

The standardized precipitation evapotranspiration index (SPEI), which was first proposed in 2010, is used to characterize the state of dry and wet climates [30]. Based on the monthly surplus and deficit of moisture, the index can comprehensively consider the effects of precipitation, evaporation, and transpiration to reasonably evaluate drought on multiple timescales. As a dry–wet index according to the potential evapotranspiration (PET) and precipitation (P), the SPEI has been widely used in drought studies worldwide. The calculation process of the SPEI is given by:

First, the cumulative series of precipitation P_i and potential evapotranspiration PET_i at different timescales are established:

$$D_n^k = \sum_{i=0}^{k-1} \left[\frac{2(i+1)}{k(k+1)} (P_{n-i} - PET_{n-i}) \right], n \geq k, \quad (1)$$

where i and k are the month and timescale (months), and n is the number of calculations. The PET is calculated following the Thornthwaite method, Penman method, etc.

Then, the log-logistic probability density function is utilized to fit the established water deficit series D , representing the difference between P and PET, and the cumulative probability for a given timescale can be calculated by the distribution function:

$$F(x) = \left[1 + \left(\frac{\alpha}{x - \gamma} \right)^\beta \right]^{-1}, \quad (2)$$

where α , β , and γ are scale, shape, and origin parameters, respectively, which can be gained from the Linear moment method.

Finally, the SPEI is obtained by transforming the fitted water deficit series to a standard normal distribution:

$$SPEI = W - \frac{C_0 + C_1W + C_2W^2}{1 + d_1W + d_2W^2 + d_3W^3}, W = \sqrt{-2\ln(P)}, \quad (3)$$

When $P \leq 0.5$, $P = 1 - F(x)$. When $P > 0.5$, $P = 1 - P$ and the sign of the SPEI is reversed. The other constants in the formula are: $C_0 = 2.515517$, $C_1 = 0.802853$, $C_2 = 0.010328$, $d_1 = 1.432788$, $d_2 = 0.189269$, and $d_3 = 0.001308$.

The principle of PDSI is the water balance equation, that is, in the case of "climatically appropriate for existing conditions", the precipitation (\hat{P}) is equal to the sum of evapotranspiration (\hat{ET}), runoff (\hat{RO}), and soil moisture exchange. The soil moisture exchange includes the soil moisture recharge (\hat{R}) and the soil moisture loss (\hat{L}). The calculation process of the PDSI is given by:

$$\hat{P} = \hat{ET} + \hat{R} + \hat{RO} - \hat{L}, \quad (4)$$

$$d = P - \hat{P} \quad (5)$$

$$Z = K_j \cdot d \quad (6)$$

$$PDSI_i = a \cdot PDSI_{i-1} + b \cdot Z_i \quad (7)$$

where \hat{P} is the monthly precipitation amount under the climatically appropriate for existing conditions; d is the water deficiency, P is the actual precipitation amount, Z is the water deficit index, and K_j is the climate correction coefficient for month j of the year. The $a = 0.897$ and $b = 1/3$ are the empirical coefficients. As a dry-wet index according to temperature and precipitation, the PDSI has been widely used in drought studies worldwide. The SPEI and PDSI values are classified as shown in Table 2 for distinguishing the drought categories [31,93]. The overall flow chart of this research is shown in Figure 2.

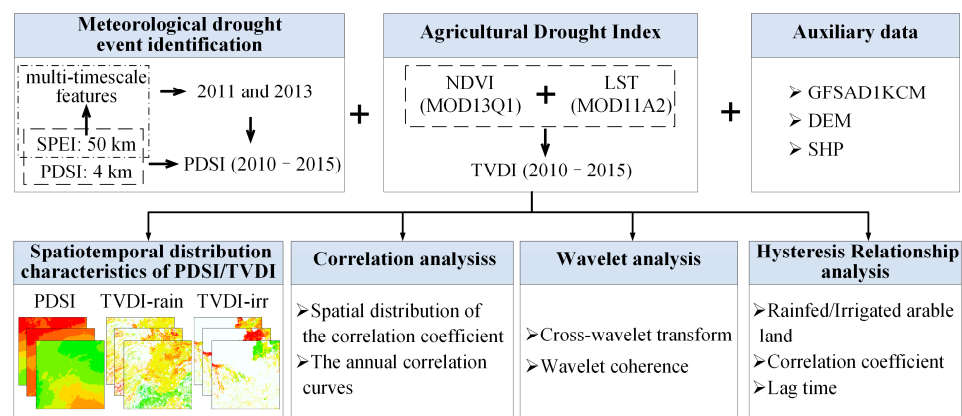


Figure 2. The flow chart of the methodology. SPEI: Standardized Precipitation Evapotranspiration Index. PDSI: Palmer Drought Severity Index. TVDI: Temperature Vegetation Drought Index. TVDI-rain/irr: TVDI of rainfed/irrigated arable land. MOD13Q1/MOD11A2: The satellite data. GFSAD1KCM: Global Food Security support Analysis Data.

Table 2. Different levels of the SPEI and PDSI.

SPEI Values	PDSI Values	Dryness/Wetness Levels
$SPEI \leq -2.0$	$PDSI \leq -4.0$	Extreme drought
$-2.0 \leq SPEI < -1.5$	$-4.0 \leq PDSI < -3.0$	Severe drought
$-1.5 \leq SPEI < -1.0$	$-3.0 \leq PDSI < -2.0$	Moderate drought
$-1.0 \leq SPEI < -0.5$	$-2.0 \leq PDSI < -1.0$	Mild drought
$-0.5 \leq SPEI < 0.5$	$-1.0 \leq PDSI < 1.0$	Normal or wet
$0.5 \leq SPEI < 1.0$	$1.0 \leq PDSI < 2.0$	Mild wet
$1.0 \leq SPEI < 1.5$	$2.0 \leq PDSI < 3.0$	Moderate wet
$1.5 \leq SPEI < 2.0$	$3.0 \leq PDSI < 4.0$	Severe wet
$SPEI \geq 2.0$	$PDSI \geq 4.0$	Extreme wet

2.3.2. Temperature Vegetation Drought Index (TVDI)

The Temperature Vegetation Drought Index (TVDI), which was proposed based on the simplified NDVI-LST two-dimensional feature space in 2002 [50], is utilized to estimate the land surface soil moisture and monitor drought:

$$TVDI = \frac{(LST - LST_{min})}{LST_{max} - LST_{min}}, \quad (8)$$

$$LST_{min} = a + b \times NDVI, \quad (9)$$

$$LST_{max} = c + d \times NDVI, \quad (10)$$

Here, NDVI is the Normalized Vegetation Index, which can reflect the physiological state of vegetation. Its calculation formula is as follows:

$$NDVI = \frac{B_{NIR} - B_R}{B_{NIR} + B_R}, \quad (11)$$

where B_{NIR} and B_R are the reflectivities in the near-infrared band and the red band, respectively.

The land surface temperature (LST) is a parameter that reflects the water shortage and soil moisture conditions during the vegetation growth period. The definition of TVDI is shown in Figure 3, according to the NDVI and LST two-dimensional spatial scatter plot. For each NDVI pixel value of a single image in the region, extracting the minimum and maximum values of the land surface temperature corresponding to each NDVI pixel (LST_{min} , LST_{max}), respectively. All LST_{min} and LST_{max} values were linearly fitted separately to obtain the wet edge and dry edge Equations (9) and (10) in the feature space, where a and c are the intercepts of the wet and dry edges, respectively, and b and d are the slopes of the wet and dry edges, respectively.

In Figure 3, the TVDI value of the pixel point P is expressed as the ratio of X and Y , where X represents the difference between the observed surface temperature of the point P and the minimum temperature expressed in Equation (9), and Y represents the difference between the maximum temperature expressed in Equation (10) and the minimum temperature at point P in this area. Therefore, the TVDI can be defined as:

$$TVDI = \frac{LST - (a + b \times NDVI)}{(c + d \times NDVI) - (a + b \times NDVI)}, \quad (12)$$

The TVDI values are negatively correlated with soil moisture, ranging from 0 to 1. When $TVDI = 1$, the pixels are on the dry edge, with the lowest soil moisture and a high degree of drought. When $TVDI = 0$, the pixels are located on the wet edge, and the soil is less affected by drought. The classification of TVDI values is shown in Table 3, according to the common division rules of TVDI values for MODIS data [10,94]. In addition, the influence of clouds needs to be considered in the TVDI calculation process. Here, this study mainly focuses on the arable land area, which accounts for about 50% of the total study area. Meanwhile, we deleted all cloud contamination pixels to calculate TVDI, and used

the inverse distance weighted interpolation method to fill the area, which greatly reduced the influence of clouds on the research results.

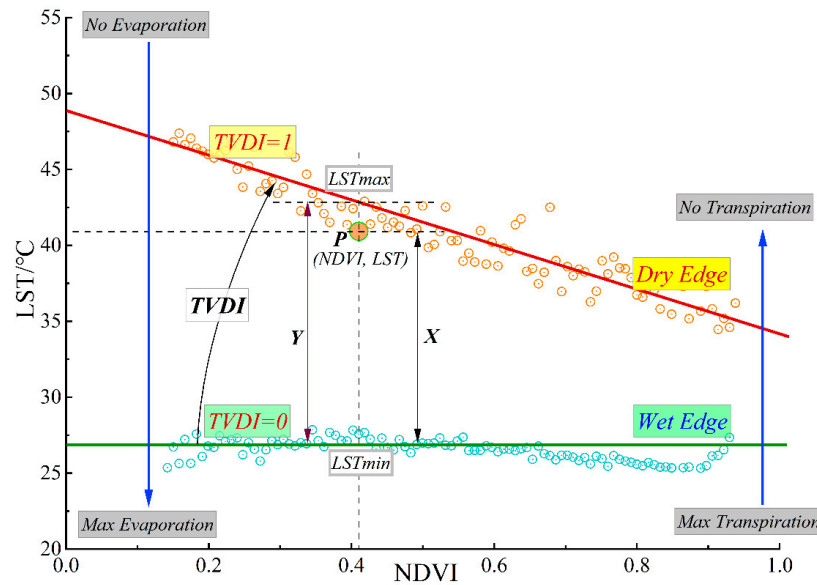


Figure 3. Definition of the Temperature Vegetation Drought Index (TVDI) and the geometric meaning of a given pixel P. Red and green circles: The maximum and minimum values (LST_{min} , LST_{max}) of LST corresponding to each NDVI pixel. Red and green lines: Dry edge and wet edge obtained from linear fitting according to all LST_{max} and LST_{min} .

Table 3. Different levels of the Temperature Vegetation Drought Index.

TVDI	Drought Levels	Soil moisture status
$0 < TVDI < 0.46$	No drought	Wet or normal land surface, no drought
$0.46 \leq TVDI < 0.57$	Mild drought	Land surface with less evaporation and near land surface with dry air
$0.57 \leq TVDI < 0.76$	Moderate drought	Dry soil surface and wilted near land surface vegetation leaves
$0.76 \leq TVDI < 0.86$	Severe drought	Thicker dry soil layers and dry vegetation
$0.86 \leq TVDI < 1$	Extreme drought	Dry or dead land surface vegetation

2.3.3. Cross-Wavelet Transform and Wavelet Coherence

A Cross-Wavelet Transform (XWT) and Wavelet Coherence (WTC) can combine time and frequency to analyze two time series datasets [74,95]. For two discrete time sequences x_n and y_n , the XWT is defined as $W^{XY} = W^X W^{Y*}$, where * indicates their complex conjugate. The cross-wavelet power is defined as $|W^{XY}|$, and the complex argument $\arg(W^{XY})$ represents the local relative phases of X_n and Y_n at the time–frequency domain. P_k^X and P_k^Y represent the cross-wavelet power and background power spectrum of the two time sequences, respectively. The theoretical formula is as follows:

$$D\left(\frac{|W_n^X(s)W_n^{Y*}(s)|}{\sigma_X\sigma_Y} < P\right) = \frac{Z_v(p)}{v} \sqrt{P_k^X P_k^Y}, \tag{13}$$

where $Z_v(p)$ is the confidence level associated with the probability p of the probability distribution function, which can be defined by the square root of two χ^2 distributions. The phase angle of the cross-wavelet is defined as:

$$\alpha = \arg(X, Y) = \arg\left[\sum_{i=1}^n \cos(\alpha_i), \sum_{i=1}^n \sin(\alpha_i)\right]. \tag{14}$$

Wavelet coherence is used to evaluate the degree of coherence of the cross-wavelet transform in the time–frequency space. It can be defined as the square of the absolute value of the smoothed cross-wavelet spectrum, normalized by the smoothed wavelet power:

$$R_n^2(s) = \frac{|S(s^{-1}W_n^{XY}(s))|^2}{S(s^{-1}|W_n^X(s)|^2) \cdot S(s^{-1}|W_n^Y(s)|^2)}, \quad (15)$$

where S is a smoothing operator:

$$S(W) = S_{scale}(S_{time}(W_n(s))), \quad (16)$$

and S_{scale} and S_{time} represent the smoothing along the wavelet scale axis and time axis, respectively. Their calculation method is as follows for the Morlet wavelet:

$$S_{scale}(W)|_n = (W_n(s) \times c_2 \Pi(0.6s))|_n, \quad (17)$$

$$S_{time}(W)|_s = (W_n(s) \times c_1 \frac{-i^2}{2s^2}) \Big|_s, \quad (18)$$

within which c_1 and c_2 are the determined normalization coefficients, and Π is the rectangle function.

2.3.4. Correlation Coefficient and Correlation Analysis

A correlation analysis is a simple statistical method for measuring the strength of the relationship between two variables and calculating their association. One of the most relevant statistical concepts is the correlation coefficient. A correlation coefficient is a unit of measurement that indicates the correlation intensity in the process of correlation analysis of variables. It is usually represented by the symbol r , having values between -1 and 1 . The closer its absolute value is to 1 , the stronger the correlation between the two variables and vice versa.

Pearson's correlation analysis can be used to examine the correlation between meteorological and agricultural drought indices [96,97]. For this study, the correlation coefficient between PDSI and TVDI in the middle and lower reaches of the Yangtze River can be calculated from two perspectives:

- (1) To explore the spatial correlation of the two indicators based on the pixel scale in 2010–2015, the formula for calculating the correlation coefficient is as follows:

$$R_{xy} = \frac{\sum_{i=1}^n [(x_i - \bar{x})(y_i - \bar{y})]}{\sqrt{\sum_{i=1}^n (x_i - \bar{x})^2} \sqrt{\sum_{i=1}^n (y_i - \bar{y})^2}}, \quad (19)$$

where R_{xy} represents the correlation coefficient between variables x and y , and x_i and y_i are the PDSI and TVDI values of the i th year, respectively. \bar{x} and \bar{y} represent the six-year average of the PDSI and TVDI, respectively.

- (2) For a pair of single-phase images, the correlation coefficients between them can be calculated by the following formula:

$$R_{ij} = \frac{\sum_{k=1}^N [(Z_{ik} - \mu_i)(Z_{jk} - \mu_j)]}{\sqrt{\sum_{k=1}^N (Z_{ik} - \mu_i)^2} \sqrt{\sum_{k=1}^N (Z_{jk} - \mu_j)^2}} \quad (20)$$

where i and j represent the PDSI and TVDI single-band images with N pixels, respectively. Z_{ik} and Z_{jk} are the values of their k th pixel, and μ_i and μ_j are the average values of the whole image pixels, respectively. The lag time between meteorological and agricultural

drought can be obtained by calculating and comparing the correlation coefficients of the two indicators on different dates.

3. Results

3.1. Meteorological Drought Event Identification

The SPEI has multi-timescale features. Figure 4 shows the interannual variations of the mean SPEI on the monthly (SPEI-1), quarterly (SPEI-3), semi-annual (SPEI-6), and one-year (SPEI-12) timescales in the middle and lower reaches of the Yangtze River from 1960 to 2015. Obviously, the SPEI frequently changes on short timescales and tends to stabilize as the timescale becomes longer. SPEI-1 shows the dry–wet state on a monthly timescale, with frequent changes and large amplitudes. SPEI-3 reflects the dry–wet changes in different seasons and is better than SPEI-1 in analyzing the annual drought conditions. However, compared with SPEI-3, on the two timescales of SPEI-6 and SPEI-12, the dry and wet changes in the study area are more obvious and gradually stabilize, which is suitable for drought monitoring over a decade. By analyzing the SPEI changes of the four timescales, the minimum SPEI values appeared in 2011 and 2013. Especially in SPEI-6 and SPEI-12, the drought situation around 2011 was particularly severe relative to recent decades. Therefore, based on the long-term SPEI monitoring in the middle and lower reaches of the Yangtze River, extreme drought events occurred in 2011 and 2013 on every time scale, further emphasizing the important research value. However, compared with the SPEI (about 50 km), the PDSI (4 km) with the higher spatial resolution is more suitable for subsequent accurate and scientific analysis of the relationship between meteorological drought and agricultural drought based on the spatial region and pixel scale. The PDSI data from 2010 to 2015 were obtained as the meteorological drought index in this research.

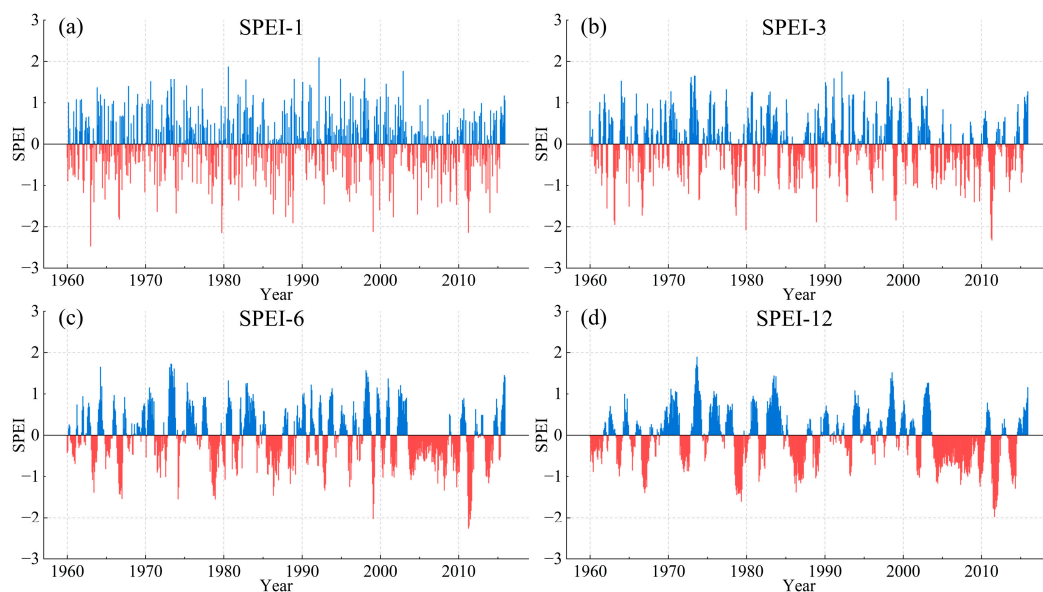


Figure 4. The interannual variations of the mean value of the SPEI on different timescales. (a) SPEI-1, (b) SPEI-3, (c) SPEI-6, and (d) SPEI-12.

3.2. Spatiotemporal Distribution Characteristics of Drought Based on the PDSI and TVDI

The response of the land surface to droughts is affected by various factors, the most important of which is the land surface moisture content. Rain-fed arable land and irrigated arable land are two significant types of agricultural land, respectively. The soil moisture of rain-fed arable land entirely depends on natural precipitation to meet the water needs of crops completely. However, artificial irrigation projects and measures are used to supplement the water for crops due to factors such as insufficient precipitation and high

temperatures throughout the year. Therefore, the two situations need to be discussed separately in the subsequent analysis.

3.2.1. Spatiotemporal Distribution Characteristics of the PDSI

According to the monthly average PDSI value in the middle and lower reaches of the Yangtze River from 2010 to 2015, the average PDSI value in 2011 was the lowest at -3.34 , followed by -1.61 in 2013, and the highest in 2015 was 0.94 (Figure 5). From March to December in 2011, the PDSI values were all lower than -2 ; this was especially the case from April to December, wherein the values were generally lower than the annual average, indicating that continuous meteorological droughts occurred in spring and summer in the study area. The drought situation in 2013 was also prominent, and the PDSI values from April to December mostly showed moderate to severe drought. Compared with 2011, the middle and lower reaches of the Yangtze River mainly experienced meteorological drought during the summer of 2013.

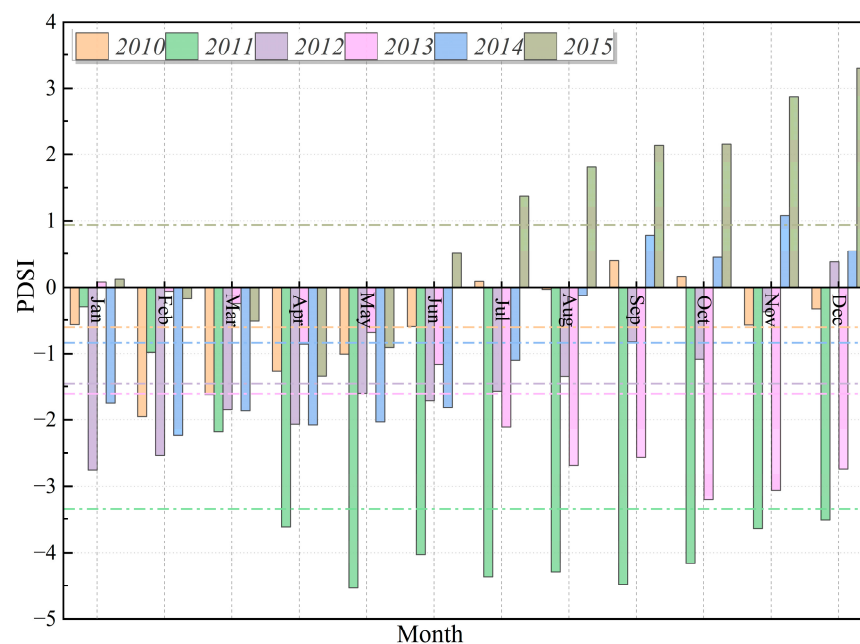


Figure 5. The monthly-averaged PDSI values of the middle and lower reaches of the Yangtze River in China from 2010 to 2015.

Figures 6 and 7 show the monthly and 3-month spatial distribution of PDSI in the middle and lower reaches of the Yangtze River in 2011 and 2013, respectively. Obviously, the meteorological drought in 2011 was more severe than in 2013. From January 2011, moderate to severe drought gradually developed in Northern Chongqing, northern Hubei, northern Anhui, and most of Guizhou and steadily spread to the south and east. The severe to extreme drought extended to almost the entire middle and lower reaches of the Yangtze River from April to May. In summer, the drought tended to subside slightly. From June to September, the severe to extreme drought was serious except for Anhui, Zhejiang, and some parts of Jiangxi. It was not until November that the meteorological drought in the middle and lower reaches of the Yangtze River was significantly relieved.

Figure 7 shows the difference more clearly in meteorological drought between the two years. Unlike the continuous drought in the spring and summer of 2011, the meteorological drought in 2013 mainly occurred in the summer. In spring, small areas in Guizhou and Hubei first experienced meteorological drought. The moderate to severe meteorological drought was observed in Southern Guizhou, most of Hubei, and Northern Chongqing in June 2013. With the rapid development of drought from July to August, severe to extreme meteorological drought occurred in most areas of Guizhou and Hubei and spread to Zhejiang and Jiangxi in September and October. The PDSI continued to show severe

meteorological drought in the northwest part of the middle and lower reaches of the Yangtze River until the end of 2013. Figure 8 shows the spatial distribution of the annual average of the PDSI in the middle and lower reaches of the Yangtze River from 2010 to 2015. The meteorological drought was the most severe in 2011. Followed by 2013 and 2012, mainly concentrated in Guizhou and Hubei. Compared with the milder drought in 2014, 2010 showed a spatial pattern of wet in the east and dry in the west. In 2015, there was almost no drought.

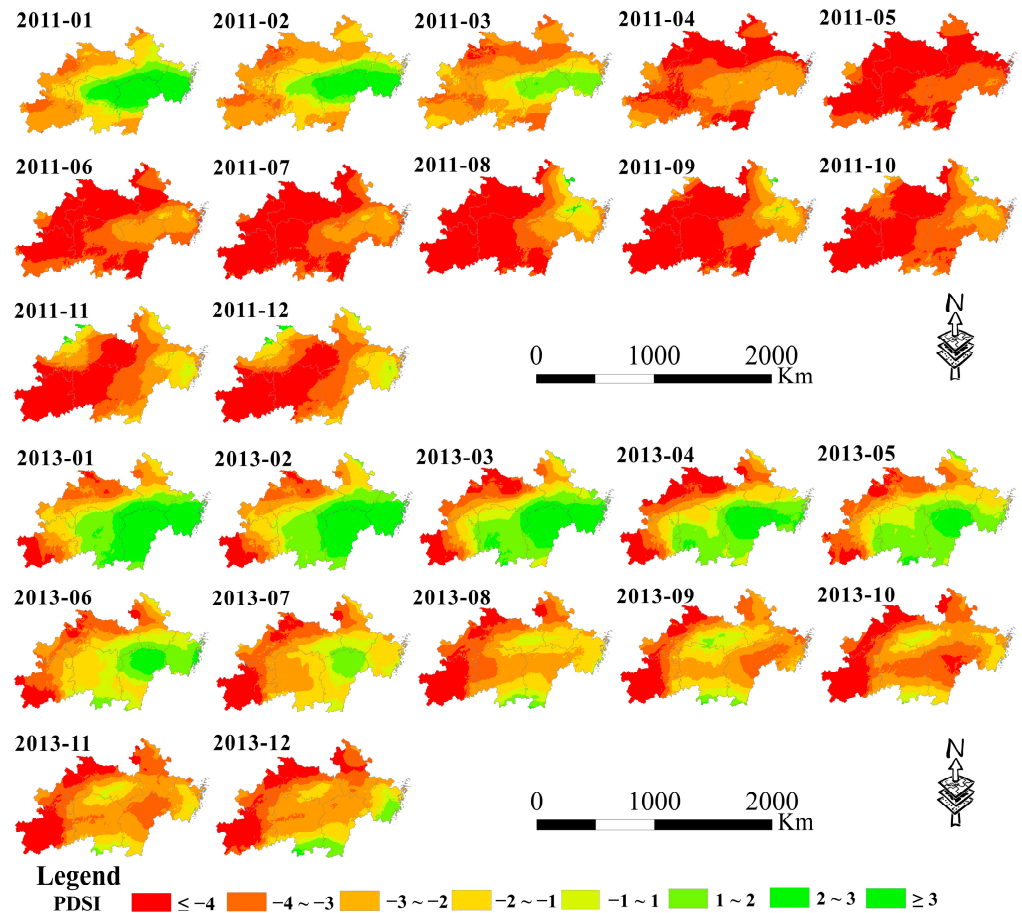


Figure 6. Monthly spatial distributions of the PDSI in the middle and lower reaches of the Yangtze River in China in 2011 and 2013.

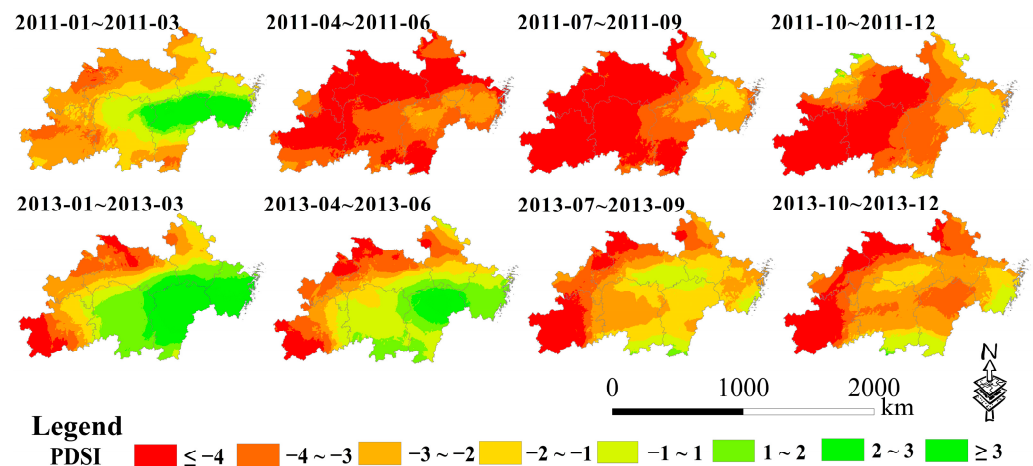


Figure 7. Spatial distributions of 3-month averages of the PDSI in the middle and lower reaches of the Yangtze River in China in 2011 and 2013.

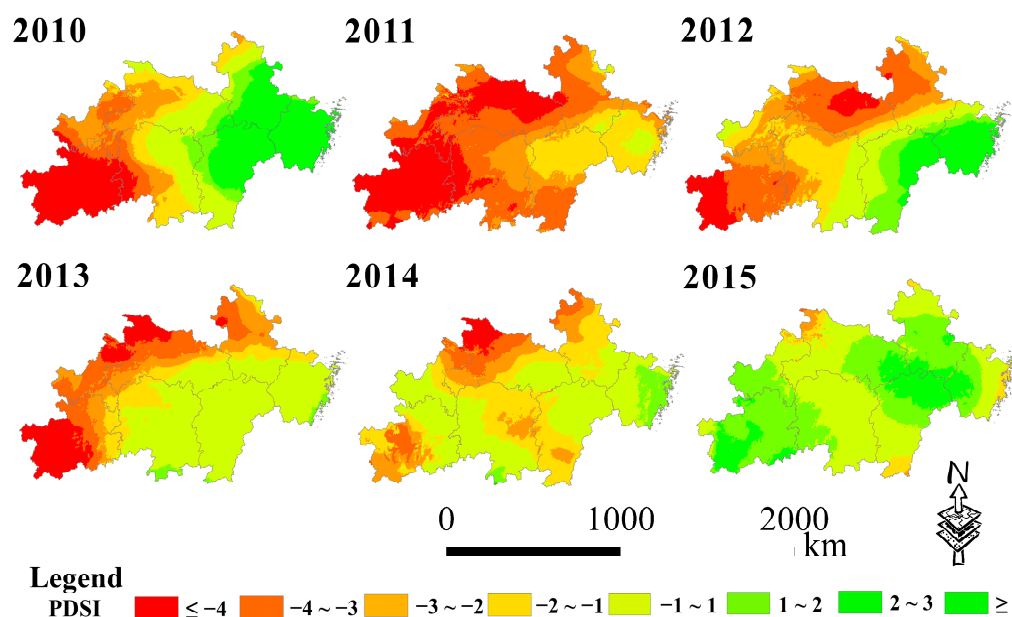


Figure 8. Spatial distributions of annual averages of the PDSI in the middle and lower reaches of the Yangtze River in China from 2010 to 2015.

3.2.2. Spatiotemporal Distribution Characteristics of TVDI

Using the two-dimensional feature space of the LST and NDVI, the dry edge and wet edge were fitted to obtain the TVDI from 2010 to 2015, which was used as the agricultural drought index in the middle and lower reaches of the Yangtze River. The TVDI of rain-fed (TVDI-rain) and irrigated arable land (TVDI-irr) were extracted separately (Figure 9). According to Figure 9, the minimum monthly average of TVDI-rain appeared in 2010 and 2015, indicating that compared with other years, the droughts in 2010 and 2015 were the lightest. Furthermore, the annual average value of TVDI-rain in 2011 was the highest at 0.699, followed by 0.689 in 2013, and the minimum value was 0.641 in 2015, indicating that the rain-fed arable land in the study area had the most severe drought in 2011 and 2013, which was consistent with the results indicated by the SPEI. Compared with TVDI-rain, the average TVDI-irr in each year from 2010–2015 is smaller than TVDI-rain, which proves that due to the existence of irrigation measures, the drought condition of irrigated arable land is weaker than that of rainfed arable land. In particular, the TVDI-irr values frequently fluctuated in 2011 and 2013, indicating that, as the meteorological drought intensified and precipitation decreased, the frequency and intensity of irrigation measures also increased. Therefore, the monthly and 3-month spatial distributions of TVDI-rain and TVDI-irr in 2011 and 2013 are shown in Figures 10–12, and the images in January and December without crop growth are removed.

Obviously, the meteorological drought developed rapidly and gradually caused the occurrence of agricultural drought due to the severe lack of precipitation and the high temperatures in the middle and lower reaches of the Yangtze River in the spring and summer of 2011 and the summer of 2013. From the end of February to the beginning of March in 2011, large-scale rain-fed crops during the planting period were in a state of moderate to severe water shortage in Guizhou, Chongqing, Hubei, and Anhui. In late March, most of the TVDI-rain values were above 0.57, and some areas reached 0.86, showing extreme drought. In April and May, the drought was relieved, in a relative sense, but western Guizhou and Chongqing were still severely dry. Compared with the rain-fed arable land, the irrigated arable land suffered much less drought. From June to August in summer, as the temperature gradually increased, severe to extreme drought conditions spread from the west to most of Hunan and Jiangxi, Central Zhejiang, and Southern Anhui. It was not until the harvest period, from the end of October to November, that the drought in the middle and lower reaches of the Yangtze River tended to disappear.

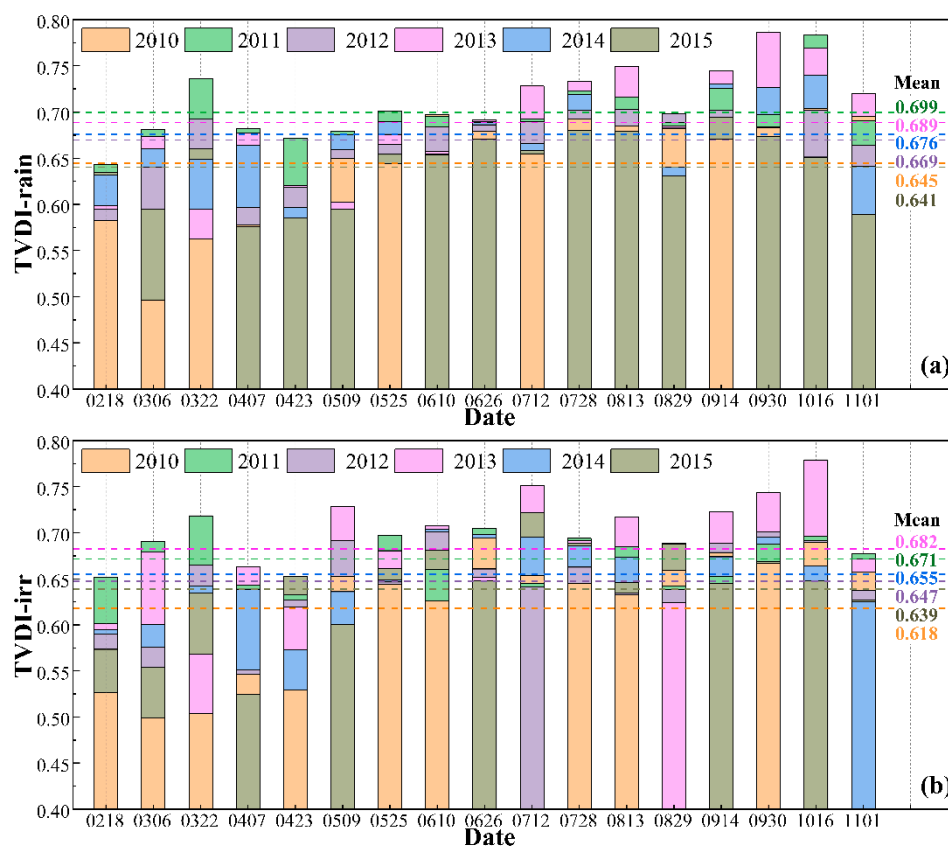


Figure 9. The average value of the TVDI in the middle and lower reaches of the Yangtze River from 2010 to 2015, with a temporal resolution of 16 days. The images without crop growth in January and December were removed. (a) The TVDI of rain-fed arable land (TVDI-rain). (b) The TVDI of irrigated arable land (TVDI-irr).

Unlike the continuous drought in the spring and summer of 2011, the drought event in the middle and lower reaches of the Yangtze River in 2013 lasted for a relatively short time. From February to June, the overall dry and wet conditions in the study area were stable, and severe drought only occurred in parts of Guizhou and Hunan in early April. In mid-to-late June, large-scale irrigated arable land was first affected by drought in Northern Anhui and Northeastern Hubei, with the TVDI reaching above 0.76 and even 0.8 in some areas, showing extreme drought. While the drought in rainfed arable land was dominant in Southern Hubei, drought in Hunan, Jiangxi, and Zhejiang did not occur until mid-July. Especially in mid-August, severe or extreme drought occurred in most areas of Guizhou and Hunan. However, the drought of irrigated arable land decreased at this time, indicating that although irrigated arable land is more sensitive to drought events, artificial irrigation can alleviate the impact of drought and establish a non-drought condition. From mid-August to early September, the drought was relieved, and the range of extreme drought was reduced due to the precipitation brought by the southwest monsoon and typhoon “Utor”. From mid-September to October, however, the drought began to intensify and expand in parts of Hunan, Jiangxi, and Zhejiang, while the drought in the middle and lower reaches of the Yangtze River continued until mid-to-late October and tended to end.

According to Figure 12a, compared with 2013, the agricultural drought of rain-fed arable land in 2011 was more severe in spring and milder in summer. However, for irrigated arable land, the degree of agricultural droughts was similar in the spring and summer of 2011 but significantly different in 2013 (Figure 12b). The results are consistent with the change in meteorological drought, proving the propagation effect from meteorological droughts to agricultural droughts. Affected by meteorology and precipitation, the response results of rain-fed arable land were consistent in different periods. However, irrigated

arable land is more sensitive to severe meteorological drought. Figure 13 shows the spatial distribution of annual average of the TVDI from 2010 to 2015. Compared with irrigated arable land, the agricultural drought degree of rainfed arable land has more obvious differences between different years. On the one hand, irrigation can significantly alleviate the stress of drought on crops and maintain a more stable dry and wet environment. On the other hand, the drought situation of rain-fed arable land is inconsistently affected by natural precipitation.

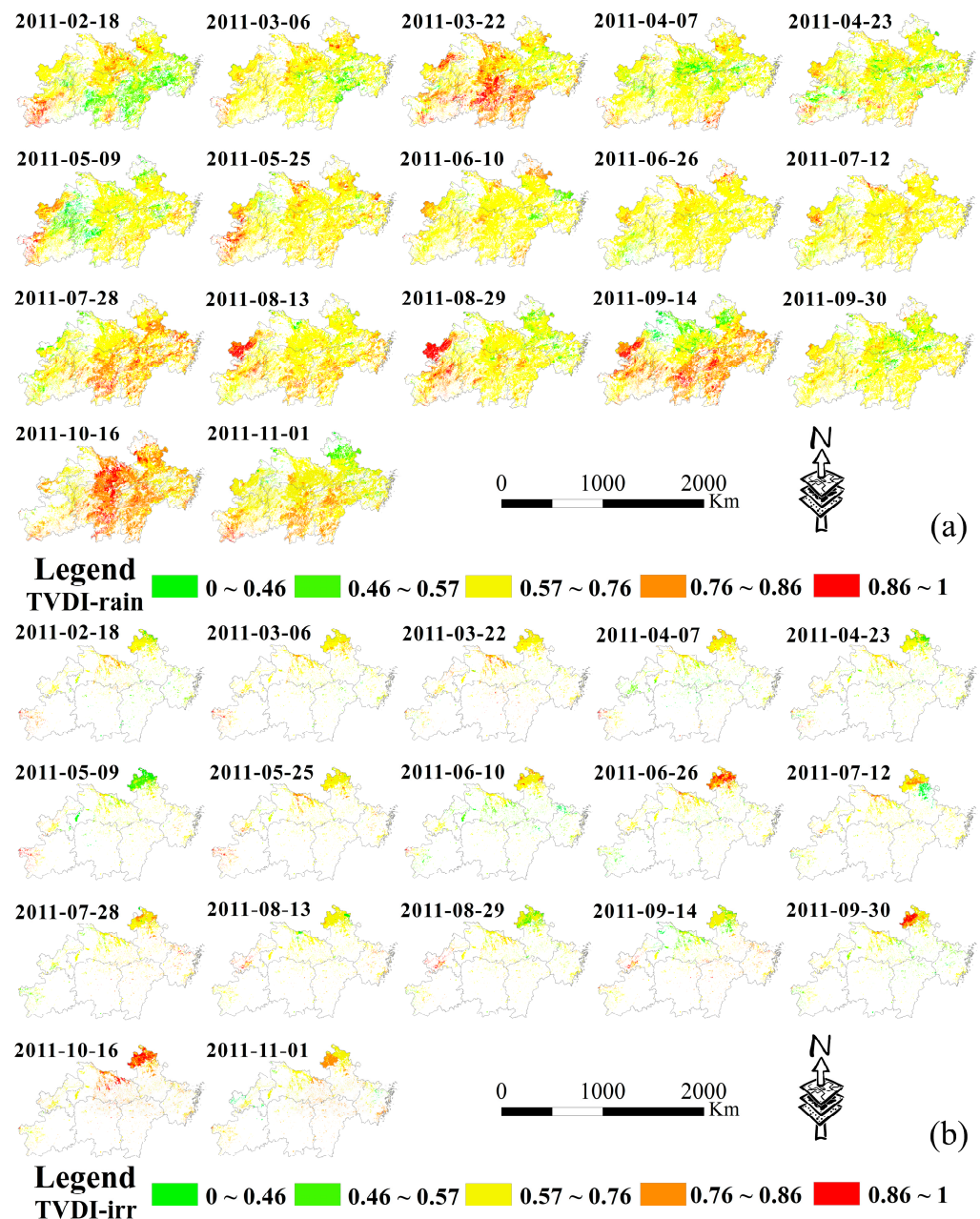


Figure 10. Spatial distribution of the Temperature Vegetation Drought Index (TVDI) in the middle and lower reaches of the Yangtze River in China in 2011, with a temporal resolution of 16 days. The images without crop growth in January and December were removed. (a) The TVDI of rain-fed arable land (TVDI-rain). (b) The TVDI of irrigated arable land (TVDI-irr).

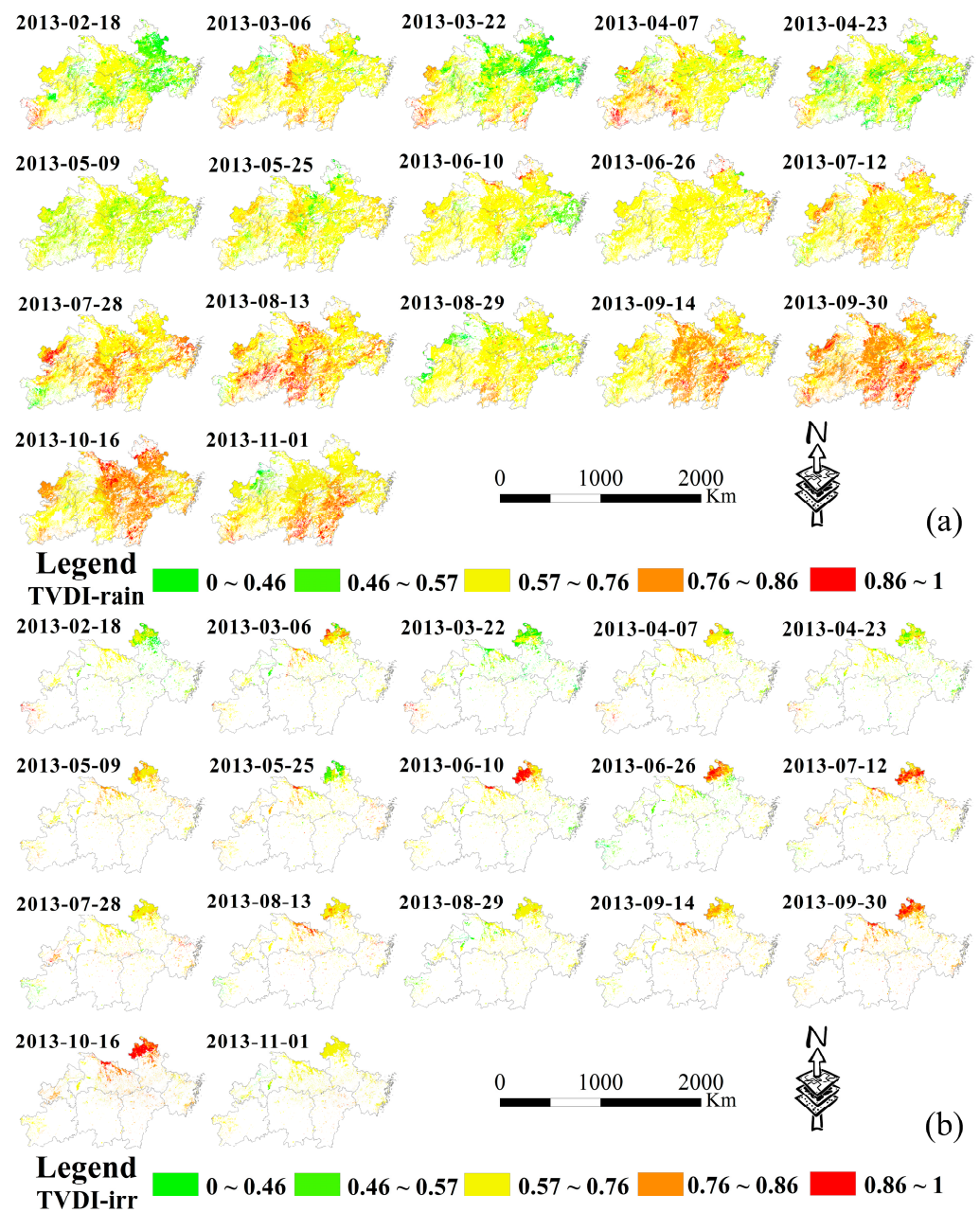


Figure 11. Spatial distribution of the Temperature Vegetation Drought Index (TVDI) in the middle and lower reaches of the Yangtze River in China in 2013, with a temporal resolution of 16 days. The images without crop growth in January and December were removed. (a) The TVDI of rain-fed arable land (TVDI-rain). (b) The TVDI of irrigated arable land (TVDI-irr).

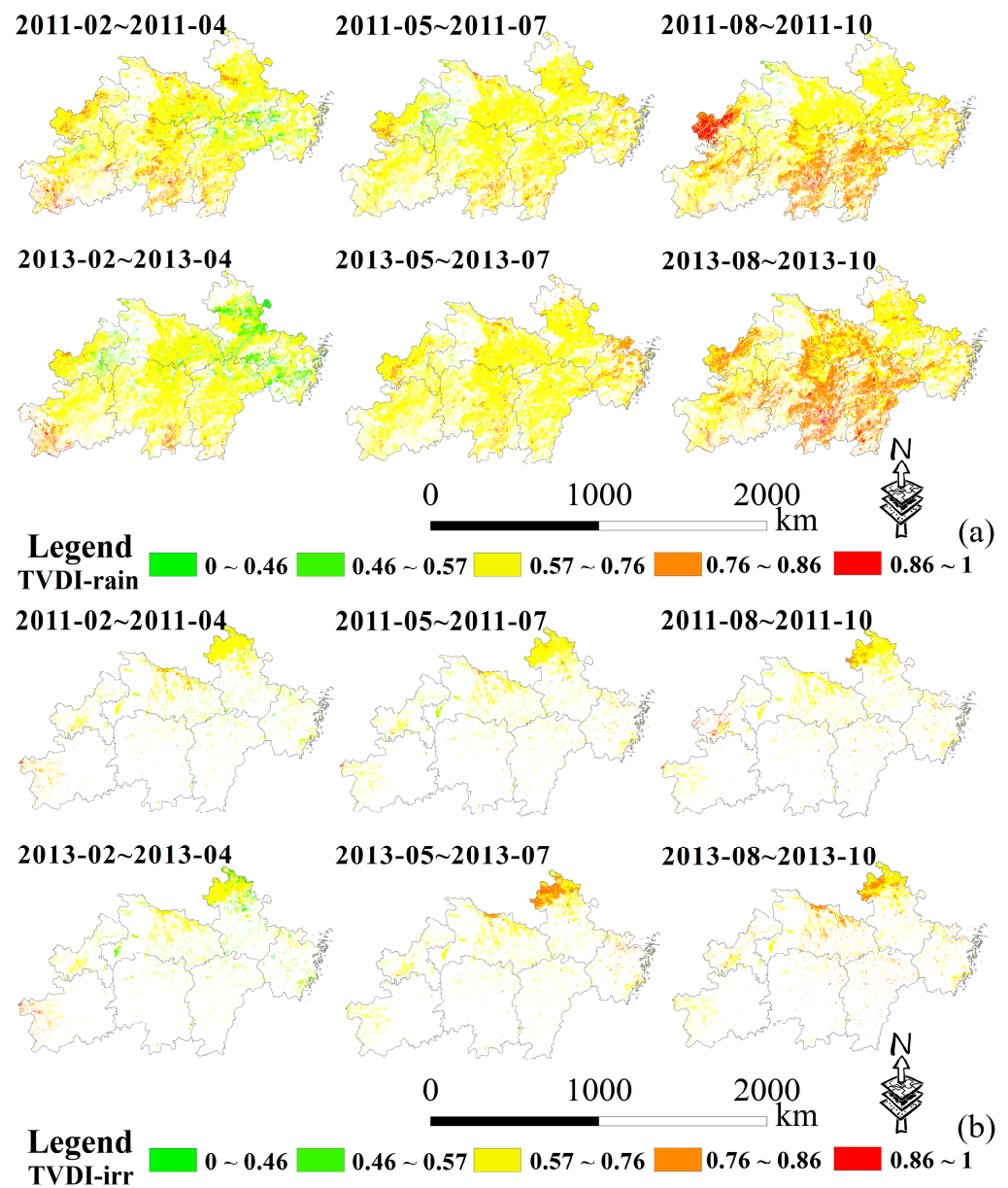


Figure 12. Spatial distribution of 3-month average of the TVDI in the middle and lower reaches of the Yangtze River in China in 2011 and 2013. The images without crop growth in January and December were removed. (a) The TVDI of rain-fed arable land (TVDI-rain). (b) The TVDI of irrigated arable land (TVDI-irr).

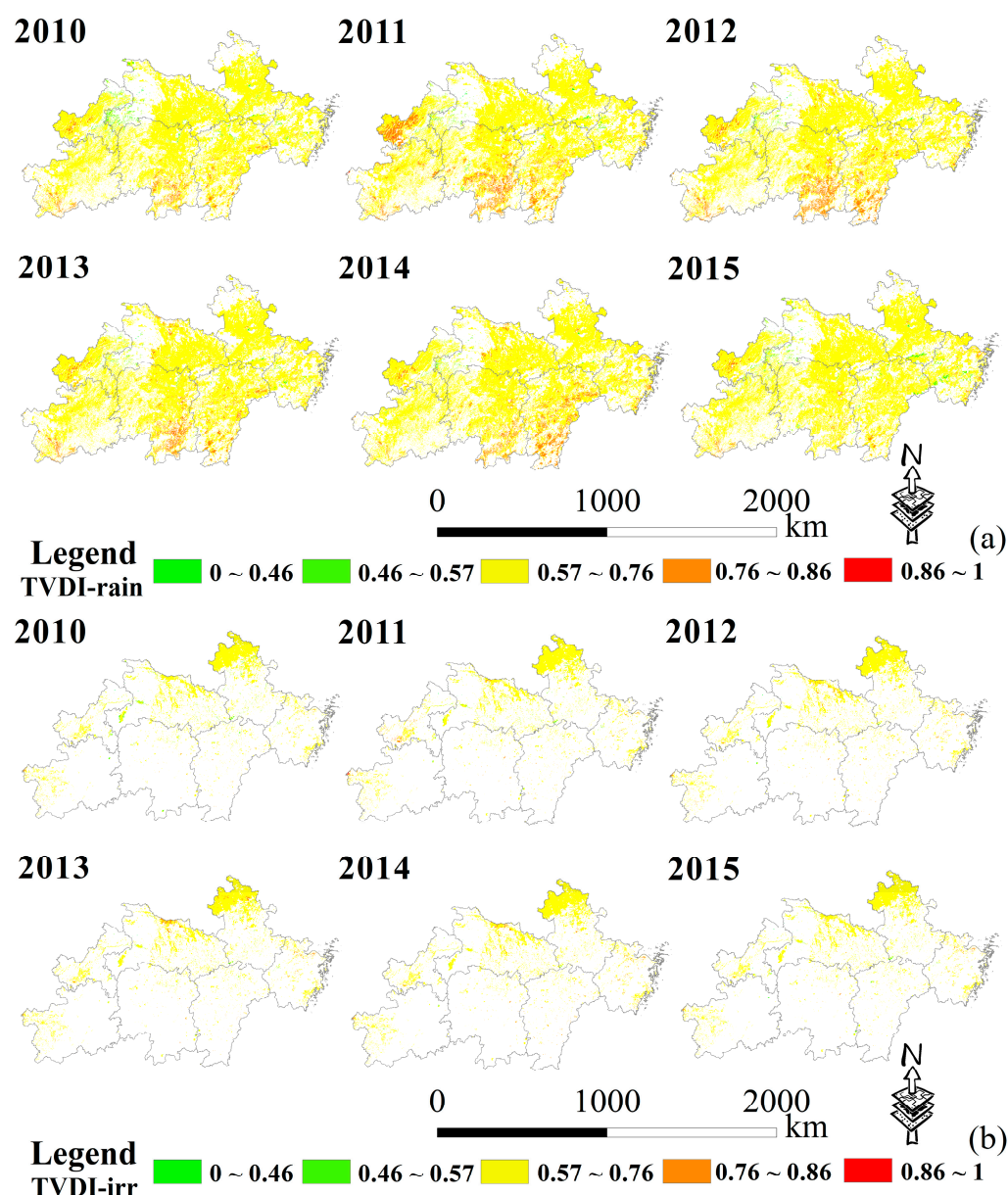


Figure 13. Spatial distribution of annual average of the TVDI in the middle and lower reaches of the Yangtze River in China from 2010 to 2015. The images without crop growth in January and December were removed. (a) The TVDI of rain-fed arable land (TVDI-rain). (b) The TVDI of irrigated arable land (TVDI-irr).

3.3. Correlation Analysis and the Lag Relationship between the PDSI and TVDI

3.3.1. Spatial Distribution of Correlation Coefficients from 2010 to 2015

Based on Equation (19), the spatial distribution of the correlation coefficient between the PDSI and TVDI based on pixel scale in the middle and lower reaches of the Yangtze River from 2010 to 2015 is shown in Figure 14. According to the statistical analysis, the spatial correlation between PDSI-rain and TVDI-rain showed an overall negative correlation. Among them, the area with a coefficient less than 0 is 414,144 square kilometers, accounting for 77.55% of the total area of rainfed arable land. The spatial correlation coefficients of PDSI-irr and TVDI-irr were positively correlated as a whole, and the area of the positive correlation region was 62,861.81 square kilometers, accounting for 68.04% of the total area of irrigated cultivated land.

Negative correlation coefficients represent opposite trends of the PDSI and TVDI, indicating that agricultural drought strongly responds to the temporal and spatial changes

in meteorology. Based on Figure 14a, the negative correlation between the two indices for 77.55% of rain-fed arable land proves that agricultural drought also occurs with the emergence of meteorological drought. On the contrary, the positive correlation between the two indices for 68.04% of irrigated arable land represents that the PDSI and TVDI have similar trends, indicating that agricultural drought did not occur or occurred later with the appearance of the meteorological drought. However, the existence of some unavoidable interference factors may affect the accuracy of the correlation coefficient in Figure 14, such as weaker meteorological droughts in other years except 2011 and 2013, and for temporal continuity, the months without vegetation growth in the study area are considered, etc.

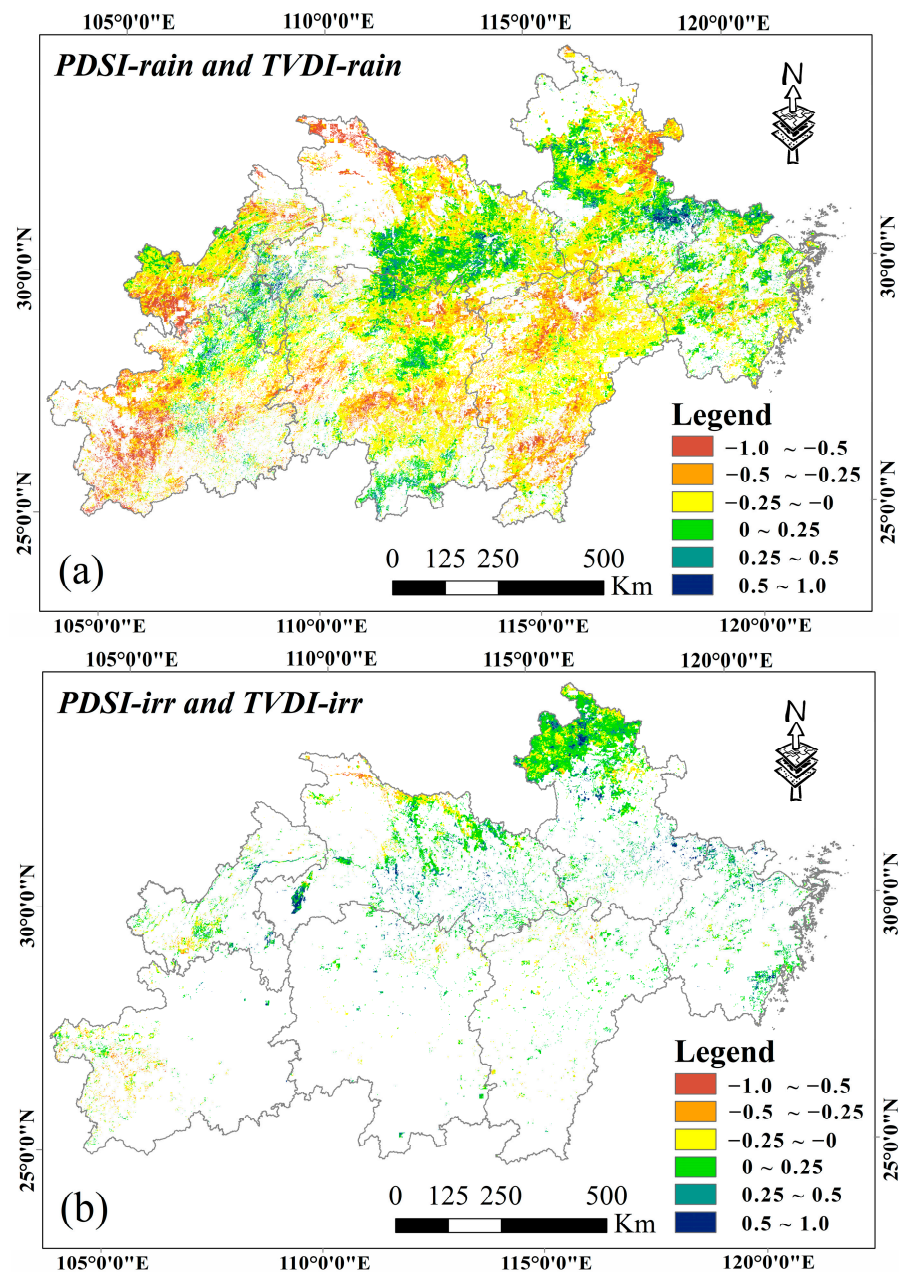


Figure 14. Spatial patterns of the correlation coefficient between the PDSI and TVDI based on annual averages in the middle and lower reaches of the Yangtze River from 2010 to 2015. Passed the significance test, with $p < 0.05$. (a) The PDSI and TVDI of rain-fed arable land. (b) The PDSI and TVDI of irrigated arable land.

The annual correlation curves between the PDSI and TVDI of rain-fed arable land and irrigated arable land in Figure 15 are more illustrative and representative, further clarifying the relationship between them. Obviously, the meteorological droughts of rain-fed arable land were negatively correlated with agricultural droughts in 2010–2015, and the correlation was most significant in 2011 and 2013. In other years, the relationship between the PDSI and TVDI was relatively weak. However, for irrigated arable land, similar to Figure 14b, the PDSI and TVDI showed different degrees of positive correlation in 2010–2015, indicating crops were less threatened by drought and grew better due to the influence of artificial irrigation measures, especially in 2010 and 2015.

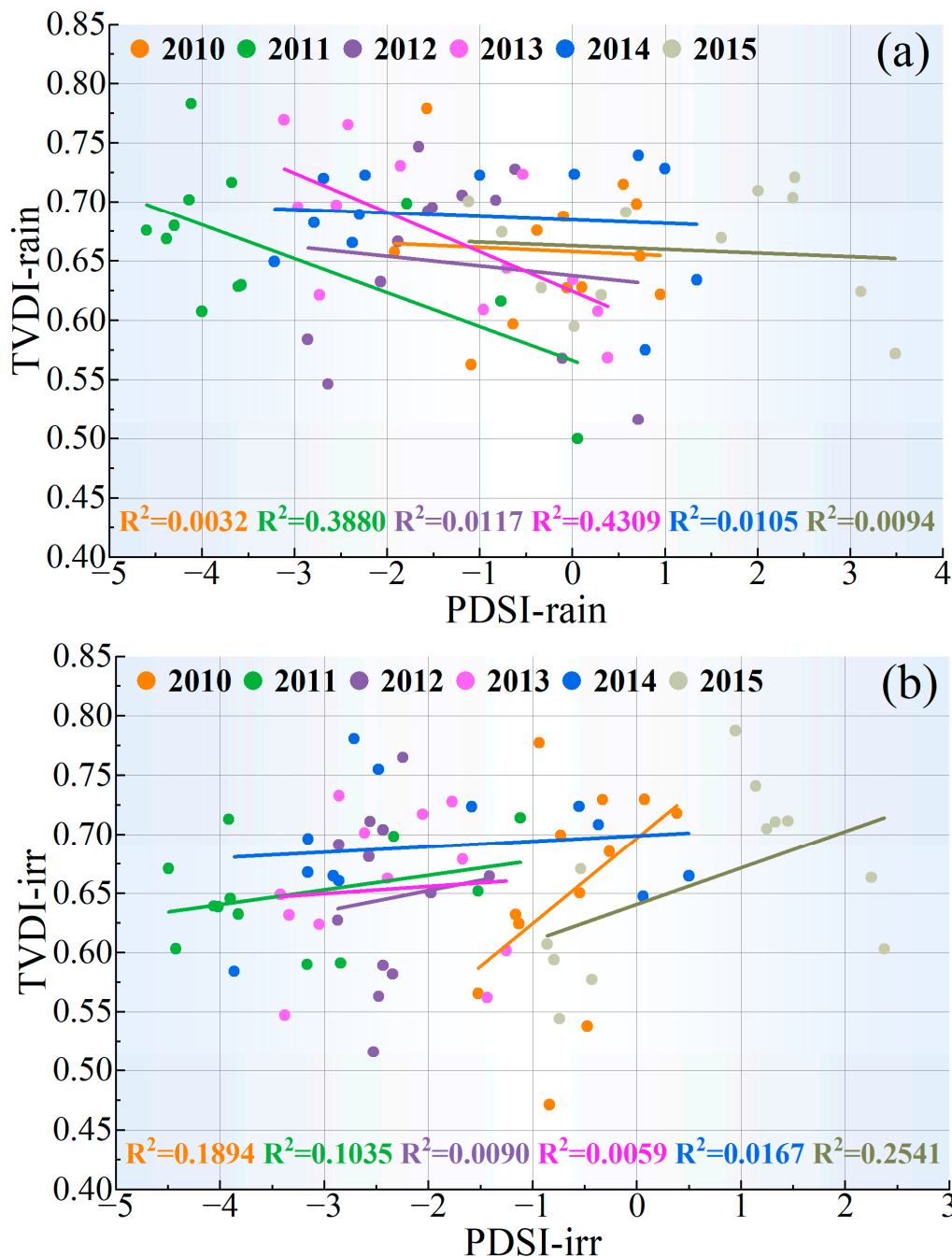


Figure 15. Correlation curves between the PDSI and TVDI of rain-fed arable land and irrigated arable land based on month averages in the middle and lower reaches of the Yangtze River from 2010 to 2015. Passed the significance test, with $p < 0.05$. (a) The correlation curves of rain-fed arable land. (b) The correlation curves of irrigated arable land.

3.3.2. Cross-Wavelet Analysis

The cross-wavelet transform and wavelet coherence were used to deduce the relationship between the PDSI and TVDI in the middle and lower reaches of the Yangtze River (Figures 16 and 17). The WTC can reflect the correlation between the PDSI and TVDI in the time–frequency domain, and XWT can analyze the lag relationship between the PDSI and TVDI data.

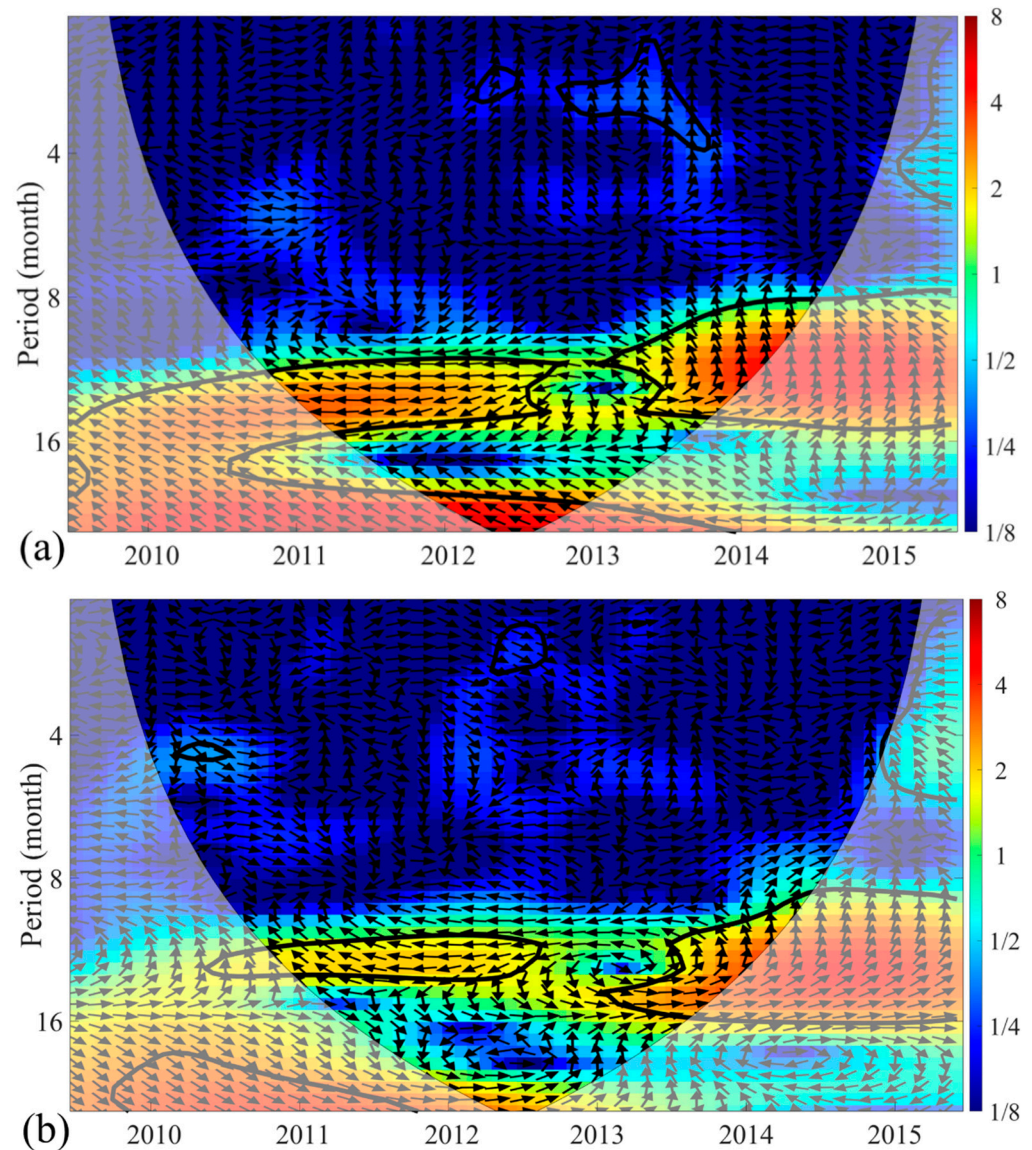


Figure 16. The cross-wavelet transform (XWT) between the PDSI and TVDI time series in the middle and lower reaches of the Yangtze River from 2010 to 2015. The abscissa and ordinate represent the year and period (month), respectively, and the color bar on the right is the wavelet energy. The arrows indicate the relative phase relationship. (a) The XWT of the PDSI and TVDI in rain-fed arable land. (b) The XWT of the PDSI and TVDI in irrigated arable land.

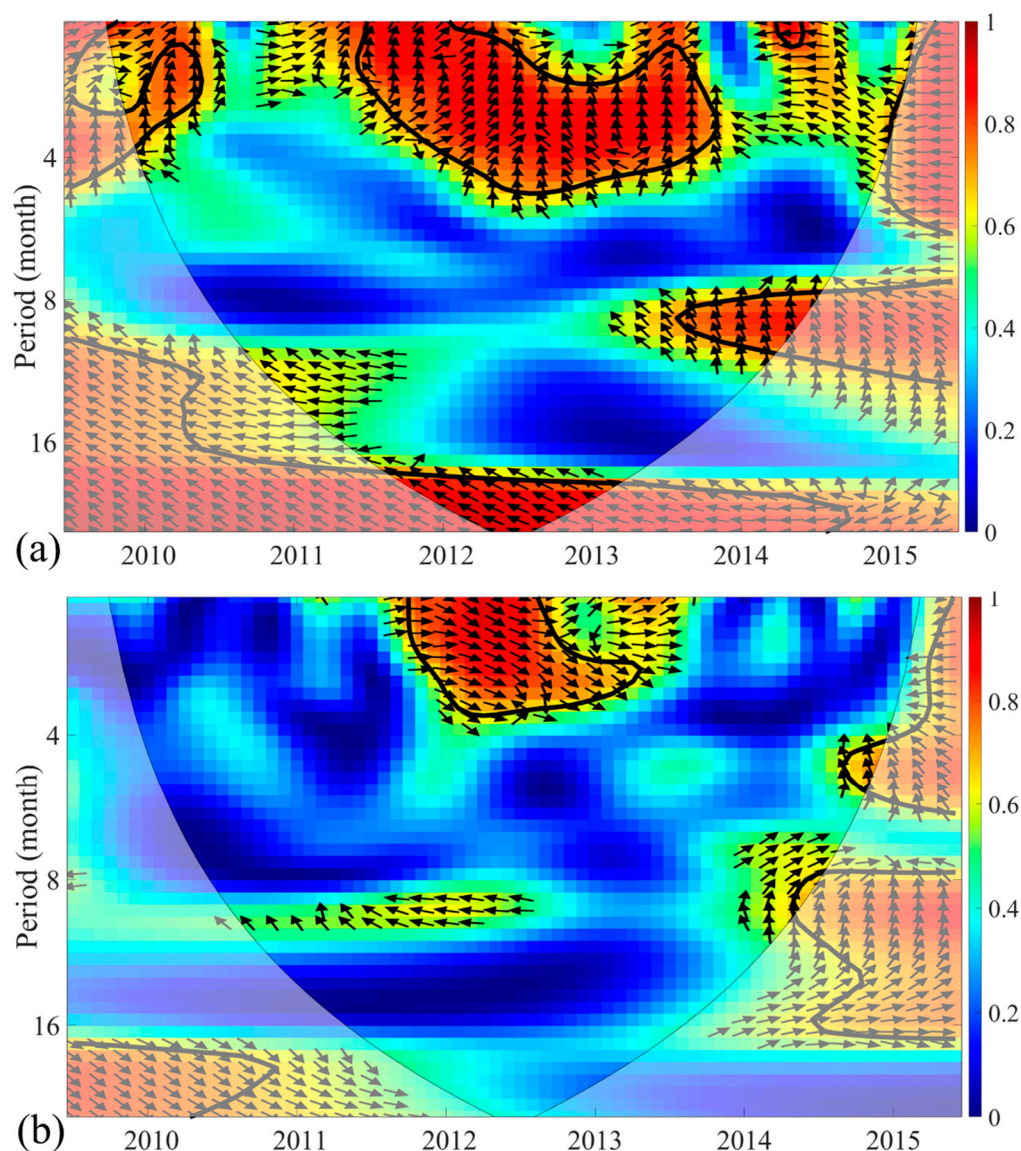


Figure 17. The wavelet coherence (WTC) between the PDSI and TVDI time series in the middle and lower reaches of the Yangtze River from 2010 to 2015. The abscissa and ordinate represent the year and period (month), respectively, and the color bar on the right is the wavelet energy. The arrows indicate the relative phase relationship. (a) The WTC of the PDSI and TVDI in rain-fed arable land. (b) The WTC of the PDSI and TVDI in irrigated arable land.

In Figures 16 and 17, the thick contour represents significance at the 95% confidence level against red noise, and the lighter black line is the cone of influence (COI) used to remove the edge effects. The wavelet energy is represented by the color bar on the right. The arrows indicate the relative phase relationship. When the PDSI and TVDI are in phase, the phase angle is 0° and the arrow points to the right, indicating that the two indicators are positively correlated. When PDSI and TVDI are in antiphase, the phase angle is 180° and the arrow points to the left, showing that the two indicators are negatively correlated.

Generally, there is a lag relationship between meteorological droughts and agricultural droughts. In the cross-wavelet transform diagram, the lag time can be calculated according to the angle pointed by the arrow. The specific calculation method of converting the phase-angle to time lag can be implemented by using MATLAB software [95]. This method has been validated and widely used in the research of the lag relationship of different time series [73,75,98,99]. In general, compared with the irrigated arable land, the PDSI and TVDI were more strongly correlated in rainfed arable land, showing a large-scale negative

correlation, especially on a 12-month timescale. By calculating the average phase angle in the XWT, the rain-fed arable land was -132.2° , indicating that agricultural drought occurs with an average lag of 33 days. However, irrigated cultivated land showed a large-scale positive correlation, and the lag time could not be determined due to the influence of irrigation measures.

3.3.3. The Correlation Coefficients between the PDSI and TVDI with Different Lag Times in 2011 and 2013

To further explore the lagged relationship between meteorological drought and agricultural drought, a correlation analysis was performed on the PDSI and TVDI for rain-fed and irrigated arable lands according to Equation (20). Based on the crop growth period and drought events in the middle and lower reaches of the Yangtze River in 2011 and 2013, the correlation coefficients between the PDSI and TVDI with different lag times were calculated (Table 4), where the lag times were determined according to the temporal resolution of the PDSI (one month) and TVDI (16 days).

Table 4. The correlation coefficients between the PDSI and TVDI.

	Lag Time	March	April	May	June	July	August	September	October	November
Rainfed croplands of PDSI and TVDI in 2011	No lag	−0.39	−0.13	−0.10	0.11	0.04	0.17	−0.26	−0.25	−0.03
	15-day lag	−0.01	−0.06	−0.41	−0.13	0.01	−0.18	−0.53	−0.36	−0.16
	30-day lag	−0.14	0.10	0.16	0.04	−0.36	−0.51	−0.09	−0.07	−0.15
	45-day lag	−0.13	0.05	0.09	0.05	−0.07	−0.03	−0.05	−0.15	−0.23
Irrigated croplands of PDSI and TVDI in 2011	No lag	−0.27	−0.06	−0.20	0.23	0.31	0.35	0.21	0.14	−0.05
	15-day lag	0.03	−0.08	−0.01	0.12	0.25	−0.03	−0.02	−0.05	0.47
	30-day lag	−0.10	0.18	0.31	0.09	0.08	0.11	0.04	0.04	−0.25
	45-day lag	−0.06	0.08	0.38	−0.07	−0.03	0.00	0.07	−0.36	−0.24
Rainfed croplands of PDSI and TVDI in 2013	No lag	−0.20	−0.21	−0.04	0.00	0.03	0.16	0.03	0.03	−0.09
	15-day lag	−0.18	−0.06	−0.17	−0.18	−0.13	−0.03	−0.22	−0.05	0.42
	30-day lag	−0.13	−0.06	−0.06	0.07	−0.30	−0.25	−0.19	−0.03	−0.01
	45-day lag	−0.01	−0.04	0.02	0.11	0.07	−0.15	0.10	0.00	0.13
Irrigated croplands of PDSI and TVDI in 2013	No lag	−0.33	−0.29	−0.08	0.12	0.29	0.30	0.20	0.13	0.11
	15-day lag	−0.21	−0.22	−0.05	−0.32	−0.09	0.12	0.09	−0.33	0.23
	30-day lag	−0.22	−0.20	−0.01	−0.17	0.08	0.12	−0.10	−0.15	0.06
	45-day lag	−0.25	0.06	−0.11	0.35	0.15	0.12	−0.24	0.25	

The lag times were determined based on the temporal resolution of the PDSI (one month) and TVDI (16 days), with $p < 0.05$ serving as the criteria to pass the significance test.

For rain-fed arable land in 2011 and 2013, the correlation between the PDSI and TVDI without lag time was relatively high during the planting and germination of vegetation from March to April in the spring, indicating that crop growth, water demand, and the dry–wet state are greatly affected by meteorological drought. In the peak season of crop development, from May to September, the PDSI was more strongly correlated with the TVDI. However, in 2011, the correlation coefficients between the PDSI and TVDI lagged by 15 days in May, June, and September and were -0.41 , -0.13 , and -0.53 , respectively. This indicates that agricultural drought occurred 15 days later than meteorological drought in these three months, while the correlation coefficient with a lag of 30 days was -0.36 and -0.51 in July and August 2011. Similarly, the crop drought in May–September 2013 lagged behind the meteorological drought by about 15 days (May, June, and September) to 30 days (July and August). In October, because of the low vegetation coverage of cultivated land caused by the autumn harvest, the correlation between the PDSI and TVDI decreased.

Similar to rain-fed arable land, there was a strong correlation between the PDSI and TVDI of irrigated arable land without a lag time in March–May in 2011 and 2013. However, the correlation in May was obviously weaker than that of rainfed arable land, with a correlation coefficient of -0.20 and -0.08 , indicating that the vegetation germination and heading stage were not significantly affected by meteorological drought due to the existence

of artificial irrigation measures. From June to October, the PDSI had a strong positive correlation with the TVDI, which was completely opposite to rainfed arable land. This was especially the case in August when the correlation coefficient reached a maximum of 0.35 and 0.30. In general, the results showed that, although an extreme meteorological drought occurred, the vegetation did not experience severe agricultural drought. On the contrary, the physiological characteristics and growth of crops were robust and consummate, proving that artificial irrigation measures and projects that supported the irrigation of cultivated land reduced or even prevented the development and occurrence of agricultural drought.

4. Discussion

Based on the severe drought events in the middle and lower reaches of the Yangtze River in the spring and summer of 2011 and the summer of 2013, the meteorological drought index, PDSI, and the agricultural drought index, TVDI, in 2010–2015 were calculated in this study. By using the methods of cross-wavelet change, wavelet coherence, and Pearson's correlation analysis, the spatiotemporal evolution patterns, correlation, and hysteresis from meteorological to agricultural droughts were analyzed and discussed for rainfed arable land and irrigated arable land. Such an analysis can support the identification and classification of drought events and guide regional agricultural activities and production.

4.1. *The Influence of Artificial Irrigation Measures on Agricultural Drought*

There is a significant response relationship between meteorological drought and agricultural drought. However, for irrigated croplands, even if severe meteorological drought occurs, artificial irrigation measures can alleviate and prevent the occurrence of agricultural drought. In this case, there may be a nonlinear relationship between meteorological drought and agricultural drought compared to rainfed arable land. Cao [79] and Zhou et al. [100] demonstrated the different responses of rainfed croplands and irrigated croplands to meteorological drought and the importance of irrigation measures. However, few studies have distinguished among them for comparative analysis. The drought-stressed area shown by the PDSI illustrates that climate change may cause soil moisture deficits, and some researchers have also proved that meteorological drought indicators play an important role in monitoring and indicating drought in irrigated arable land [101–103], but it does not consider the realities of agricultural production processes. The TVDI can describe the actual agricultural drought conditions due to the combination of the LST and NDVI. Therefore, we should fully consider the differences between rainfed and irrigated arable land types when exploring the relationship between meteorological and agricultural drought, especially in the critical stage of crop growth. The results in Section 3.3 serve to demonstrate further the significance of this study in distinguishing between the two types of croplands.

4.2. *The Significance of Hysteresis Analysis of Agricultural Drought*

The propagation time of meteorological drought to agricultural drought can be understood as the lag time of agricultural drought to meteorological drought. Thus, this study discussed the hysteresis relationship between meteorological drought and agricultural drought by combining cross-wavelet change and Pearson's correlation analysis. The maximum correlation coefficient method based on Pearson's correlation analysis can judge the spread of drought, but most studies concentrated on the propagation process of meteorological drought to hydrological drought [104–106]. In fact, the spread of meteorological drought to agricultural drought is more complex [12], and accurate monitoring of the lag time is also particularly important.

In Section 3.3.3, the time with the largest correlation coefficient was taken as the lag time of agricultural drought. The results showed that the lag of rain-fed cultivated land is prominent, while the lag relationship of irrigated cultivated land is not obvious. The main reason for the lag relationship is that the intervention of artificial irrigation measures prevented the propagation of meteorological drought to agricultural drought. Zhou

et al. [100] also found that the propagation time from meteorological drought to agricultural drought was shorter under drier conditions than in the case of wetter conditions, which was confirmed by the results of this paper, and further clarifies the significance of analyzing the hysteresis based on rain-irrigated cultivated land.

4.3. The Limitations of this Study

There are some limitations and deficiencies in this research:

(1) Only a single agricultural drought index TVDI and a single meteorological drought index, the PDSI, were selected in this research, and there was no comparative analysis between different indices. In addition, the PDSI is more commonly used for drought analysis on large time scales. Decades of PDSI and TVDI data can be supplemented for subsequent long-term drought studies. Furthermore, various remote sensing or meteorological drought indices can be used to compare and analyze the actual conditions of different drought types or regions. There are differences in the drought monitoring effect of special indicators. Despite that drought classification levels are only used to analyze the overall development of drought, the uncertainty caused by the classification still needs to be considered seriously. In fact, few researchers have investigated the applicability of existing drought indices under different drought regimes in different regions. Therefore, further research needs to combine multiple drought indices to improve the accuracy of drought monitoring. (2) There was a lack of comprehensive consideration for the sensitivity of different vegetation species to the TVDI and PDSI due to the differences in the growth periods of crops. Therefore, the study area can be further subdivided according to the crop planting range. When combined with the index monitoring results, the analysis of both the drought conditions and their causes can be more accurately portrayed.

(3) The representativeness of the classification base map of rainfed and irrigated cultivated land has not been verified, and the quality of the base map will greatly affect the accuracy of various indicators in subsequent research. Therefore, it is necessary to carefully select the arable land classification maps. The comparison of various datasets and the accurate distribution information of irrigated arable cropland become the primary objective of the next research paper.

5. Conclusions

With an increasing global warming trend, monitoring drought disasters has become particularly scientific and persistent. This is especially the case for agricultural droughts, which seriously threaten agricultural production and food security. Therefore, monitoring and predicting agricultural drought events represent a significant and lasting subject. As a large-scale data source, satellite remote sensing data provide strong support for identifying and analyzing drought disasters. The proposal of multiple drought indices can make it easier to analyze the temporal and spatial evolution of drought scientifically. The PDSI and TVDI were selected as the meteorological and agricultural drought indices for the study, and the major conclusions are as follows:

(1) According to the SPEI monitoring on different time scales in the middle and lower reaches of the Yangtze River for several decades, extreme drought events occurred in 2011 and 2013. Meanwhile, in order to improve the accuracy, high-resolution PDSI data is more appropriate for meteorological drought monitoring and meets the needs of this study. Moreover, the monitoring results show that severe to extreme meteorological drought occurred in different spatial ranges in the middle and lower reaches of the Yangtze River in the spring and summer of 2011 and the summer of 2013, which is consistent with the records of drought events, indicating the feasibility of using the PDSI for multi-year meteorological drought monitoring.

(2) In the summer of 2011, the rain-fed arable land of the study area featured prominent agricultural drought, and severe to extreme droughts gradually spread from the west to most of Hunan and Jiangxi, Central Zhejiang, and Southern Anhui. In addition, large areas of irrigated arable land experienced drought first in mid-to-late June of 2013, such as

Northern Anhui and Northeastern Hubei. One month later, the rain-fed arable land, mainly in Southern Hubei, Hunan, Jiangxi, and Zhejiang, suffered from agricultural drought. Compared with rainfed land, drought has a greater impact on irrigated land, indicating that irrigated lands are more sensitive to drought. However, artificial irrigation measures and projects have a certain ability to control droughts, which can alleviate the growth-related stress of drought on vegetation. Due to the high drought sensitivity of irrigated land, therefore, it is necessary for water conservancy and agricultural departments to accurately predict and judge the agricultural drought that may be caused by meteorological drought and ensure the timeliness and accuracy of irrigation measures to protect food security. The effect of irrigation in preventing and mitigating drought is beneficial for disaster management decision-making and can be instructive for developing and implementing disaster reduction schemes.

(3) There is a certain lag relationship between the occurrence of meteorological droughts and agricultural droughts. The average lag time from meteorological to agricultural droughts in the middle and lower reaches of the Yangtze River from 2010 to 2015 was 33 days. For rain-fed arable land, compared with meteorological drought, the occurrence of agricultural drought was delayed by 0–30 days during the entire growth period of vegetation. This is especially the case in the key season of vegetation growth from May to September, when there is a one-month lag between agricultural drought and meteorological drought. On the contrary, the SPEI and TVDI of irrigated arable land were positively correlated from June to October, further indicating that irrigated arable land was not threatened by drought due to the existence of irrigation measures and projects. Therefore, under the stress of meteorological drought, timely drought prevention measures, especially the water supplement for irrigated arable land crops, can ensure food security and improve the sustainability of local water resource management. For rainfed arable land, it can also provide policymakers with a scientific basis for drought mitigation strategies, such as increasing and expanding irrigation measures.

Author Contributions: Conceptualization, F.C. and H.J.; methodology, E.D.; software, E.D.; validation, E.D. and H.J.; formal analysis, E.D.; writing—original draft preparation, E.D.; writing—review and editing, F.C., H.J., L.W. and A.Y.; visualization, E.D.; supervision, F.C. and H.J.; project administration, F.C., H.J. and L.W.; and funding acquisition, F.C., H.J., L.W. and A.Y. All authors have read and agreed to the published version of the manuscript.

Funding: This research was funded by the China-ASEAN Big Earth Data Platform and Applications (CADA, guikeAA20302022) and the National Natural Science Foundation of China (42171078).

Data Availability Statement: Not applicable.

Conflicts of Interest: The authors declare no conflict of interest.

References

1. Orimoloye, I.R.; Belle, J.A.; Olusola, A.O.; Busayo, E.T.; Ololade, O.O. Spatial assessment of drought disasters, vulnerability, severity and water shortages: A potential drought disaster mitigation strategy. *Nat. Hazards* **2021**, *105*, 2735–2754. [[CrossRef](#)]
2. Hisdal, H.; Tallaksen, L.M. Estimation of regional meteorological and hydrological drought characteristics: A case study for Denmark. *J. Hydrol.* **2003**, *281*, 230–247. [[CrossRef](#)]
3. Poonia, V.; Jha, S.; Goyal, M.K. Copula based analysis of meteorological, hydrological and agricultural drought characteristics across Indian river basins. *Int. J. Climatol.* **2021**, *41*, 4637–4652. [[CrossRef](#)]
4. Ma, B.; Zhang, B.; Jia, L.; Huang, H. Conditional distribution selection for SPEI-daily and its revealed meteorological drought characteristics in China from 1961 to 2017. *Atmos. Res.* **2020**, *246*, 105108. [[CrossRef](#)]
5. Guan, X.; Zang, Y.; Meng, Y.; Liu, Y.; Lv, H.; Yan, D. Study on spatiotemporal distribution characteristics of flood and drought disaster impacts on agriculture in China. *Int. J. Disaster Risk Reduct.* **2021**, *64*, 102504. [[CrossRef](#)]
6. Ahmad, M.M.; Yaseen, M.; Saqib, S.E. Climate change impacts of drought on the livelihood of dryland smallholders: Implications of adaptation challenges. *Int. J. Disaster Risk Reduct.* **2022**, *80*, 103210. [[CrossRef](#)]
7. West, H.; Quinn, N.; Horswell, M. Remote sensing for drought monitoring & impact assessment: Progress, past challenges and future opportunities. *Remote Sens. Environ.* **2019**, *232*, 111291.
8. Jia, H.; Chen, F.; Zhang, C.; Dong, J.; Du, E.; Wang, L. High emissions could increase the future risk of maize drought in China by 60–70%. *Sci. Total Environ.* **2022**, *852*, 158474. [[CrossRef](#)]

9. Wilhite, D.A.; Glantz, M.H. Understanding: The drought phenomenon: The role of definitions. *Water Int.* **1985**, *10*, 111–120. [[CrossRef](#)]
10. He, Y.; Chen, F.; Jia, H.; Wang, L.; Bondur, V.G. Different drought legacies of rain-fed and irrigated croplands in a typical Russian agricultural region. *Remote Sens.* **2020**, *12*, 1700. [[CrossRef](#)]
11. Darcup, J.; Lee, K.; Paulson, E. On the definition of drought. *Water Resour. Res.* **1980**, *16*, 297–302. [[CrossRef](#)]
12. Leng, G.; Tang, Q.; Rayburg, S. Climate change impacts on meteorological, agricultural and hydrological droughts in China. *Glob. Planet. Chang.* **2015**, *126*, 23–34. [[CrossRef](#)]
13. Wang, D.; Hejazi, M.; Cai, X.; Valocchi, A.J. Climate change impact on meteorological, agricultural, and hydrological drought in central Illinois. *Water Resour. Res.* **2011**, *47*, W09527. [[CrossRef](#)]
14. Wang, W.; Ertsen, M.W.; Svoboda, M.D.; Hafeez, M. Propagation of Drought: From Meteorological Drought to Agricultural and Hydrological Drought. *Adv. Meteorol.* **2016**, *2016*, 6547209. [[CrossRef](#)]
15. Wu, Z.; Mao, Y.; Li, X.; Lu, G.; Lin, Q.; Xu, H. Exploring spatiotemporal relationships among meteorological, agricultural, and hydrological droughts in Southwest China. *Stoch. Environ. Res. Risk Assess.* **2016**, *30*, 1033–1044. [[CrossRef](#)]
16. Ding, Y.; Gong, X.; Xing, Z.; Cai, H.; Zhou, Z.; Zhang, D.; Sun, P.; Shi, H. Attribution of meteorological, hydrological and agricultural drought propagation in different climatic regions of China. *Agric. Water Manag.* **2021**, *255*, 106996. [[CrossRef](#)]
17. Salimi, H.; Asadi, E.; Darbandi, S. Meteorological and hydrological drought monitoring using several drought indices. *Appl. Water Sci.* **2021**, *11*, 11. [[CrossRef](#)]
18. Araneda-Cabrera, R.J.; Bermúdez, M.; Puertas, J. Benchmarking of drought and climate indices for agricultural drought monitoring in Argentina. *Sci. Total Environ.* **2021**, *790*, 148090. [[CrossRef](#)]
19. Chen, F.; Wang, N.; Yu, B.; Wang, L. Res2-Unet, a new deep architecture for building detection from high spatial resolution images. *IEEE J. Sel. Top. Appl. Earth Obs. Remote Sens.* **2022**, *15*, 1494–1501. [[CrossRef](#)]
20. Javed, T.; Li, Y.; Rashid, S.; Li, F.; Hu, Q.; Feng, H.; Chen, X.; Ahmad, S.; Liu, F.; Pulatov, B. Performance and relationship of four different agricultural drought indices for drought monitoring in China’s mainland using remote sensing data. *Sci. Total Environ.* **2021**, *759*, 143530. [[CrossRef](#)]
21. Wei, W.; Zhang, J.; Zhou, J.; Zhou, L.; Xie, B.; Li, C. Monitoring drought dynamics in China using Optimized Meteorological Drought Index (OMDI) based on remote sensing data sets. *J. Environ. Manag.* **2021**, *292*, 112733. [[CrossRef](#)] [[PubMed](#)]
22. Lemma, E.; Upadhyaya, S.; Ramsankaran, R. Meteorological drought monitoring across the main river basins of Ethiopia using satellite rainfall product. *Environ. Syst. Res.* **2022**, *11*, 7. [[CrossRef](#)]
23. Neeti, N.; Murali, C.A.; Chowdary, V.; Rao, N.; Kesarwani, M. Integrated meteorological drought monitoring framework using multi-sensor and multi-temporal earth observation datasets and machine learning algorithms: A case study of central India. *J. Hydrol.* **2021**, *601*, 126638. [[CrossRef](#)]
24. Shahzaman, M.; Zhu, W.; Ullah, I.; Mustafa, F.; Bilal, M.; Ishfaq, S.; Nisar, S.; Arshad, M.; Iqbal, R.; Aslam, R.W. Comparison of multi-year reanalysis, models, and satellite remote sensing products for agricultural drought monitoring over south asian countries. *Remote Sens.* **2021**, *13*, 3294. [[CrossRef](#)]
25. Wei, W.; Zhang, J.; Zhou, L.; Xie, B.; Zhou, J.; Li, C. Comparative evaluation of drought indices for monitoring drought based on remote sensing data. *Environ. Sci. Pollut. Res.* **2021**, *28*, 20408–20425. [[CrossRef](#)]
26. Yu, B.; Xu, C.; Chen, F.; Wang, N.; Wang, L. HADeenNet: A hierarchical-attention multi-scale deconvolution network for landslide detection. *Int. J. Appl. Earth Obs. Geoinf.* **2022**, *111*, 102853. [[CrossRef](#)]
27. Cheval, S. The standardized precipitation index—an overview. *Rom. J. Meteorol.* **2015**, *12*, 17–64.
28. Yuan, W.-P.; Zhou, G.-S. Comparison between standardized precipitation index and Z-index in China. *Chin. J. Plant Ecol.* **2004**, *28*, 523.
29. GB/T 20481-2017; Grades of Meteorological Drought. CMA: Beijing, China, 2017.
30. Vicente-Serrano, S.M.; Beguería, S.; López-Moreno, J.I. A multiscalar drought index sensitive to global warming: The standardized precipitation evapotranspiration index. *J. Clim.* **2010**, *23*, 1696–1718. [[CrossRef](#)]
31. Yu, H.; Zhang, Q.; Xu, C.-Y.; Du, J.; Sun, P.; Hu, P. Modified palmer drought severity index: Model improvement and application. *Environ. Int.* **2019**, *130*, 104951. [[CrossRef](#)]
32. Zhou, Y.; Zhou, P.; Jin, J.; Wu, C.; Cui, Y.; Zhang, Y.; Tong, F. Drought identification based on Palmer drought severity index and return period analysis of drought characteristics in Huaibei Plain China. *Environ. Res.* **2022**, *212*, 113163. [[CrossRef](#)] [[PubMed](#)]
33. Dai, A. Characteristics and trends in various forms of the Palmer Drought Severity Index during 1900–2008. *J. Geophys. Res. Atmos.* **2011**, *116*, D12115. [[CrossRef](#)]
34. Wardlow, B.; Anderson, M.; Verdin, J. *Remote Sensing of Drought: Innovative Monitoring Approaches*; CRC Press: Boca Raton, FL, USA, 2012.
35. Hayes, M.J.; Svoboda, M.D.; Wardlow, B.D.; Anderson, M.C.; Kogan, F. Drought monitoring: Historical and current perspectives. In *Remote Sensing of Drought: Innovative Monitoring Approaches*; CRC Press: Boca Raton, FL, USA, 2012; pp. 1–19.
36. Alahacoon, N.; Edirisinghe, M. A comprehensive assessment of remote sensing and traditional based drought monitoring indices at global and regional scale. *Geomat. Nat. Hazards Risk* **2022**, *13*, 762–799. [[CrossRef](#)]
37. Liu, X.; Zhu, X.; Pan, Y.; Li, S.; Liu, Y.; Ma, Y. Agricultural drought monitoring: Progress, challenges, and prospects. *J. Geogr. Sci.* **2016**, *26*, 750–767. [[CrossRef](#)]
38. Zhai, J.; Su, B.; Krysanova, V.; Vetter, T.; Gao, C.; Jiang, T. Spatial variation and trends in PDSI and SPI indices and their relation to streamflow in 10 large regions of China. *J. Clim.* **2010**, *23*, 649–663. [[CrossRef](#)]

39. Yiping, L.; Yaohui, L. Advances in adaptability of meteorological drought indices in China. *J. Arid Meteorol.* **2017**, *35*, 709.
40. Zhao, H.; Gao, G.; An, W.; Zou, X.; Li, H.; Hou, M. Timescale differences between SC-PDSI and SPEI for drought monitoring in China. *Phys. Chem. Earth Parts A/B/C* **2017**, *102*, 48–58. [[CrossRef](#)]
41. Yan, H.; Wang, S.Q.; Wang, J.B.; Lu, H.Q.; Guo, A.H.; Zhu, Z.C.; Myneni, R.B.; Shugart, H.H. Assessing spatiotemporal variation of drought in China and its impact on agriculture during 1982–2011 by using PDSI indices and agriculture drought survey data. *J. Geophys. Res. Atmos.* **2016**, *121*, 2283–2298. [[CrossRef](#)]
42. Zhang, M.; Chen, F.; Guo, H.; Yi, L.; Zeng, J.; Li, B. Glacial Lake Area Changes in High Mountain Asia during 1990–2020 Using Satellite Remote Sensing. *Research* **2022**, *2022*, 9821275. [[CrossRef](#)]
43. Tang, F.; Wang, L.; Guo, Y.; Fu, M.; Huang, N.; Duan, W.; Luo, M.; Zhang, J.; Li, W.; Song, W. Spatio-temporal variation and coupling coordination relationship between urbanisation and habitat quality in the Grand Canal, China. *Land Use Policy* **2022**, *117*, 106119. [[CrossRef](#)]
44. Yu, B.; Yang, A.; Chen, F.; Wang, N.; Wang, L. SNNFD, spiking neural segmentation network in frequency domain using high spatial resolution images for building extraction. *Int. J. Appl. Earth Obs. Geoinf.* **2022**, *112*, 102930. [[CrossRef](#)]
45. Chen, F.; Zhang, M.; Guo, H.; Allen, S.; Kargel, J.S.; Haritashya, U.K.; Watson, C.S. Annual 30 m dataset for glacial lakes in High Mountain Asia from 2008 to 2017. *Earth Syst. Sci. Data* **2021**, *13*, 741–766. [[CrossRef](#)]
46. Tucker, C.J. Red and photographic infrared linear combinations for monitoring vegetation. *Remote Sens. Environ.* **1979**, *8*, 127–150. [[CrossRef](#)]
47. Huete, A.; Didan, K.; Miura, T.; Rodriguez, E.P.; Gao, X.; Ferreira, L.G. Overview of the radiometric and biophysical performance of the MODIS vegetation indices. *Remote Sens. Environ.* **2002**, *83*, 195–213. [[CrossRef](#)]
48. Bento, V.A.; Gouveia, C.M.; DaCamara, C.C.; Libonati, R.; Trigo, I.F. The roles of NDVI and Land Surface Temperature when using the Vegetation Health Index over dry regions. *Glob. Planet. Chang.* **2020**, *190*, 103198. [[CrossRef](#)]
49. Bento, V.A.; Gouveia, C.M.; DaCamara, C.C.; Trigo, I.F. A climatological assessment of drought impact on vegetation health index. *Agric. For. Meteorol.* **2018**, *259*, 286–295. [[CrossRef](#)]
50. Sandholt, I.; Rasmussen, K.; Andersen, J. A simple interpretation of the surface temperature/vegetation index space for assessment of surface moisture status. *Remote Sens. Environ.* **2002**, *79*, 213–224. [[CrossRef](#)]
51. Li, Z.; Tan, D. The second modified perpendicular drought index (MPDI1): A combined drought monitoring method with soil moisture and vegetation index. *J. Indian Soc. Remote Sens.* **2013**, *41*, 873–881. [[CrossRef](#)]
52. Ghulam, A.; Qin, Q.; Teyip, T.; Li, Z.-L. Modified perpendicular drought index (MPDI): A real-time drought monitoring method. *ISPRS J. Photogramm. Remote Sens.* **2007**, *62*, 150–164. [[CrossRef](#)]
53. Rao, M.; Silber-Coats, Z.; Powers, S.; Fox III, L.; Ghulam, A. Mapping drought-impacted vegetation stress in California using remote sensing. *GISci. Remote Sens.* **2017**, *54*, 185–201. [[CrossRef](#)]
54. Ghulam, A.; Qin, Q.; Zhan, Z. Designing of the perpendicular drought index. *Environ. Geol.* **2007**, *52*, 1045–1052. [[CrossRef](#)]
55. Zhang, H.; Chen, H.; Shen, S.; Zou, C. The application of Modified Perpendicular Drought Index (MPDI) method in drought remote sensing monitoring. In Proceedings of the Remote Sensing and Modeling of Ecosystems for Sustainability, San Diego, CA, USA, 10 September 2008; pp. 286–294.
56. Kogan, F.N. Application of vegetation index and brightness temperature for drought detection. *Adv. Space Res.* **1995**, *15*, 91–100. [[CrossRef](#)]
57. Bayarjargal, Y.; Karnieli, A.; Bayasgalan, M.; Khudulmur, S.; Gandush, C.; Tucker, C. A comparative study of NOAA–AVHRR derived drought indices using change vector analysis. *Remote Sens. Environ.* **2006**, *105*, 9–22. [[CrossRef](#)]
58. Jackson, R.D.; Reginato, R.; Idso, S. Wheat canopy temperature: A practical tool for evaluating water requirements. *Water Resour. Res.* **1977**, *13*, 651–656. [[CrossRef](#)]
59. Moran, M.; Clarke, T.; Inoue, Y.; Vidal, A. Estimating crop water deficit using the relation between surface-air temperature and spectral vegetation index. *Remote Sens. Environ.* **1994**, *49*, 246–263. [[CrossRef](#)]
60. Valipour, M. Use of surface water supply index to assessing of water resources management in Colorado and Oregon, US. *Adv. Agric. Sci. Eng. Res.* **2013**, *3*, 631–640.
61. Garen, D.C. Revised surface-water supply index for western United States. *J. Water Resour. Plan. Manag.* **1993**, *119*, 437–454. [[CrossRef](#)]
62. Doesken, N.J.; McKee, T.B.; Kleist, J.D. *Development of a Surface Water Supply Index for the Western United States*; Climatology Report 91-3; Colorado State University: Fort Collins, CO, USA, 1991.
63. Haboudane, D.; Miller, J.R.; Pattey, E.; Zarco-Tejada, P.J.; Strachan, I.B. Hyperspectral vegetation indices and novel algorithms for predicting green LAI of crop canopies: Modeling and validation in the context of precision agriculture. *Remote Sens. Environ.* **2004**, *90*, 337–352. [[CrossRef](#)]
64. Bachmair, S.; Stahl, K.; Collins, K.; Hannaford, J.; Acreman, M.; Svoboda, M.; Knutson, C.; Smith, K.H.; Wall, N.; Fuchs, B. Drought indicators revisited: The need for a wider consideration of environment and society. *Wiley Interdiscip. Rev. Water* **2016**, *3*, 516–536. [[CrossRef](#)]
65. Wan, W.; Liu, Z.; Li, J.; Xu, J.; Wu, H.; Xu, Z. Spatiotemporal patterns of maize drought stress and their effects on biomass in the Northeast and North China Plain from 2000 to 2019. *Agric. For. Meteorol.* **2022**, *315*, 108821. [[CrossRef](#)]

66. Du, L.; Song, N.; Liu, K.; Hou, J.; Hu, Y.; Zhu, Y.; Wang, X.; Wang, L.; Guo, Y. Comparison of two simulation methods of the temperature vegetation dryness index (TVDI) for drought monitoring in semi-arid regions of China. *Remote Sens.* **2017**, *9*, 177. [[CrossRef](#)]
67. Liang, L.; ZHAO, S.-H.; QIN, Z.-H.; HE, K.-X.; Chong, C.; LUO, Y.-X.; ZHOU, X.-D. Drought change trend using MODIS TVDI and its relationship with climate factors in China from 2001 to 2010. *J. Integr. Agric.* **2014**, *13*, 1501–1508. [[CrossRef](#)]
68. Shashikant, V.; Mohamed Shariff, A.R.; Wayayok, A.; Kamal, M.R.; Lee, Y.P.; Takeuchi, W. Utilizing TVDI and NDWI to classify severity of agricultural drought in Chuping, Malaysia. *Agronomy* **2021**, *11*, 1243. [[CrossRef](#)]
69. Weidan, W.; Li, S.; Zhiyuan, P.; Yuanyuan, C.; Mo, D. Comparison of TVDI and soil moisture response based on various vegetation indices. In Proceedings of the 2021 9th International Conference on Agro-Geoinformatics (Agro-Geoinformatics), Shenzhen, China, 26–29 July 2021; pp. 1–5.
70. Seidenfaden, I.K.; Jensen, K.H.; Sonnenborg, T.O. Climate change impacts and uncertainty on spatiotemporal variations of drought indices for an irrigated catchment. *J. Hydrol.* **2021**, *601*, 126814.
71. Kuśmierk-Tomaszewska, R.; Żarski, J. Assessment of Meteorological and Agricultural Drought Occurrence in Central Poland in 1961–2020 as an Element of the Climatic Risk to Crop Production. *Agriculture* **2021**, *11*, 855. [[CrossRef](#)]
72. Behrang Manesh, M.; Khosravi, H.; Heydari Alamdarloo, E.; Saadi Alekasir, M.; Gholami, A.; Singh, V.P. Linkage of agricultural drought with meteorological drought in different climates of Iran. *Theor. Appl. Climatol.* **2019**, *138*, 1025–1033. [[CrossRef](#)]
73. Du, C.; Chen, J.; Nie, T.; Dai, C. Spatial–temporal changes in meteorological and agricultural droughts in Northeast China: Change patterns, response relationships and causes. *Nat. Hazards* **2022**, *110*, 155–173. [[CrossRef](#)]
74. Li, R.; Chen, N.; Zhang, X.; Zeng, L.; Wang, X.; Tang, S.; Li, D.; Niyogi, D. Quantitative analysis of agricultural drought propagation process in the Yangtze River Basin by using cross wavelet analysis and spatial autocorrelation. *Agric. For. Meteorol.* **2020**, *280*, 107809. [[CrossRef](#)]
75. Tian, Q.; Lu, J.; Chen, X. A novel comprehensive agricultural drought index reflecting time lag of soil moisture to meteorology: A case study in the Yangtze River basin, China. *Catena* **2022**, *209*, 105804. [[CrossRef](#)]
76. Hu, C.; Zhao, L.; Wang, Y.; Xue, X.; Wu, L. Analysis of the relationship between the meteorological, agriculture and hydrological drought. *Meteorol. Environ. Sci.* **2016**, *39*, 1–6.
77. Li, Y.; Huang, S.; Wang, H.; Zheng, X.; Huang, Q.; Deng, M.; Peng, J. High-resolution propagation time from meteorological to agricultural drought at multiple levels and spatiotemporal scales. *Agric. Water Manag.* **2022**, *262*, 107428. [[CrossRef](#)]
78. Alahacoon, N.; Edirisinghe, M.; Ranagalage, M. Satellite-based meteorological and agricultural drought monitoring for agricultural sustainability in Sri Lanka. *Sustainability* **2021**, *13*, 3427. [[CrossRef](#)]
79. Cao, S.; Zhang, L.; He, Y.; Zhang, Y.; Chen, Y.; Yao, S.; Yang, W.; Sun, Q. Effects and contributions of meteorological drought on agricultural drought under different climatic zones and vegetation types in Northwest China. *Sci. Total Environ.* **2022**, *821*, 153270. [[CrossRef](#)] [[PubMed](#)]
80. Li, M.; Chai, X.; Wang, G.; Hu, W.; Zhang, L. Research on meteorological drought in the middle and lower reaches of the Yangtze River. *Nat. Resour.* **2019**, *34*, 374–384. [[CrossRef](#)]
81. Qin, P.; Liu, M. Methods for diagnosis and assessment of meteorological drought and application in the middle and lower Yangtze Basin. *Resour. Environ. Yangtze Basin* **2015**, *24*, 1969–1976.
82. Yin, G.; Zhang, H.; Zhang, L. Remote Sensing Monitoring of Agricultural Drought and Vegetation Sensitivity Analysis in the Middle and Lower Reaches of the Yangtze River from 2001 to 2019. *Geomat. Inf. Sci. Wuhan Univ.* **2022**, *47*, 1245–1256.
83. Siqi, W.; Xiang, Z.; Nengcheng, C.; Jiayang, Z.; Chuli, H.; Xiaoting, P. Monitoring and comparison of drought in five provinces of the middle and lower reaches of the Yangtze River based on the multiple drought indices. *J. Arid Meteorol.* **2019**, *37*, 209.
84. Jia, H.; Chen, F.; Pan, D.; Du, E.; Wang, L.; Wang, N.; Yang, A. Flood risk management in the Yangtze River basin—Comparison of 1998 and 2020 events. *Int. J. Disaster Risk Reduct.* **2022**, *68*, 102724. [[CrossRef](#)]
85. Jia, H.; Chen, F.; Zhang, J.; Du, E. Vulnerability analysis to drought based on remote sensing indexes. *Int. J. Environ. Res. Public Health* **2020**, *17*, 7660. [[CrossRef](#)]
86. Teluguntla, P.; Thenkabail, P.S.; Xiong, J.; Gumma, M.K.; Giri, C.; Milesi, C.; Ozdogan, M.; Congalton, R.; Tilton, J.; Sankey, T.T. Global Cropland Area Database (GCAD) derived from remote sensing in support of food security in the twenty-first century: Current achievements and future possibilities. In *Land Resources Monitoring, Modeling, and Mapping with Remote Sensing (Remote Sensing Handbook)*; CAB Direct: Boca Raton, FL, USA, 2015; pp. 1–19.
87. Gumma, M.; Thenkabail, P.; Teluguntla, P.; Oliphant, A.; Xiong, J.; Congalton, R.; Yadav, K.; Smith, C. NASA Making Earth System Data Records for Use in Research Environments (MEASURES) Global Food Security-Support Analysis Data (GFSAD) Cropland Extent 2015 South Asia, Afghanistan, Iran 30 m v001. In *NASA EOSDIS Land Processes DAAC*; USGS: Sioux Falls, SD, USA, 2017.
88. Teluguntla, P.; Thenkabail, P.S.; Xiong, J.; Gumma, M.K.; Giri, C.; Milesi, C.; Ozdogan, M.; Congalton, R.G.; Tilton, J. Global food security support analysis data (GFSAD) at nominal 1 km (GCAD) derived from remote sensing in support of food security in the twenty-first century: Current achievements and future possibilities. In *Land Resources Monitoring, Modeling, and Mapping with Remote Sensing*; CRC Press: Boca Raton, FL, USA, 2015; pp. 131–160.
89. Yadav, K.; Congalton, R.G. Accuracy assessment of global food security-support analysis data (GFSAD) cropland extent maps produced at three different spatial resolutions. *Remote Sens.* **2018**, *10*, 1800. [[CrossRef](#)]

90. Angulo Martínez, M.; Beguería, S.; El-Kenawy, A.; López-Moreno, J.; Vicente Serrano, S. The SPEIbase: A new gridded product for the analysis of drought variability and drought impacts. In Proceedings of the European Conference on Applied Climatology (ECAC) & European Meteorological Society (EMS), Lodz, Poland, 10–14 September 2010.
91. Vicente-Serrano, S.M.; Beguería, S.; López-Moreno, J.I.; Angulo, M.; El Kenawy, A. A new global 0.5 gridded dataset (1901–2006) of a multiscalar drought index: Comparison with current drought index datasets based on the Palmer Drought Severity Index. *J. Hydrometeorol.* **2010**, *11*, 1033–1043. [[CrossRef](#)]
92. Abatzoglou, J.T.; Dobrowski, S.Z.; Parks, S.A.; Hegewisch, K.C. TerraClimate, a high-resolution global dataset of monthly climate and climatic water balance from 1958–2015. *Sci. Data* **2018**, *5*, 170191. [[CrossRef](#)] [[PubMed](#)]
93. Deng, H.; Cheng, F.; Wang, J.; Wang, C. Monitoring of Drought in Central Yunnan, China Based on TVDI Model. *Pol. J. Environ. Stud.* **2021**, *30*, 3511–3523. [[CrossRef](#)]
94. Wu, L. Classification of drought grades based on temperature vegetation drought index using the MODIS data. *Res. Soil Water Conserv.* **2017**, *24*, 130–135.
95. Grinsted, A.; Moore, J.C.; Jevrejeva, S. Application of the cross wavelet transform and wavelet coherence to geophysical time series. *Nonlinear Process. Geophys.* **2004**, *11*, 561–566. [[CrossRef](#)]
96. Sedgwick, P. Pearson's correlation coefficient. *BMJ Br. Med. J.* **2012**, *345*, e4483. [[CrossRef](#)]
97. Ly, A.; Marsman, M.; Wagenmakers, E.J. Analytic posteriors for Pearson's correlation coefficient. *Stat. Neerl.* **2018**, *72*, 4–13. [[CrossRef](#)]
98. Li, Q.; He, P.; He, Y.; Han, X.; Zeng, T.; Lu, G.; Wang, H. Investigation to the relation between meteorological drought and hydrological drought in the upper Shaying River Basin using wavelet analysis. *Atmos. Res.* **2020**, *234*, 104743. [[CrossRef](#)]
99. Gao, C.; Chen, C.; He, Y.; Ruan, T.; Luo, G.; Sun, Y. Response of Agricultural Drought to Meteorological Drought: A Case Study of the Winter Wheat above the Bengbu Sluice in the Huaihe River Basin, China. *Water* **2020**, *12*, 2805. [[CrossRef](#)]
100. Zhou, K.; Li, J.; Zhang, T.; Kang, A. The use of combined soil moisture data to characterize agricultural drought conditions and the relationship among different drought types in China. *Agric. Water Manag.* **2021**, *243*, 106479. [[CrossRef](#)]
101. Dash, S.S.; Sahoo, B.; Raghuvanshi, N.S. A SWAT-Copula based approach for monitoring and assessment of drought propagation in an irrigation command. *Ecol. Eng.* **2019**, *127*, 417–430. [[CrossRef](#)]
102. Mondol, M.A.H.; Zhu, X.; Dunkerley, D.; Henley, B.J. Changing occurrence of crop water surplus or deficit and the impact of irrigation: An analysis highlighting consequences for rice production in Bangladesh. *Agric. Water Manag.* **2022**, *269*, 107695. [[CrossRef](#)]
103. Meliho, M.; Khattabi, A.; Jobbins, G.; Sghir, F. Impact of meteorological drought on agriculture in the Tensift watershed of Morocco. *J. Water Clim. Chang.* **2020**, *11*, 1323–1338. [[CrossRef](#)]
104. Zhou, Z.; Shi, H.; Fu, Q.; Ding, Y.; Li, T.; Wang, Y.; Liu, S. Characteristics of propagation from meteorological drought to hydrological drought in the Pearl River Basin. *J. Geophys. Res. Atmos.* **2021**, *126*, e2020JD033959. [[CrossRef](#)]
105. Bhardwaj, K.; Shah, D.; Aadhar, S.; Mishra, V. Propagation of meteorological to hydrological droughts in India. *J. Geophys. Res. Atmos.* **2020**, *125*, e2020JD033455. [[CrossRef](#)]
106. Ding, Y.; Xu, J.; Wang, X.; Cai, H.; Zhou, Z.; Sun, Y.; Shi, H. Propagation of meteorological to hydrological drought for different climate regions in China. *J. Environ. Manag.* **2021**, *283*, 111980. [[CrossRef](#)] [[PubMed](#)]

Disclaimer/Publisher's Note: The statements, opinions and data contained in all publications are solely those of the individual author(s) and contributor(s) and not of MDPI and/or the editor(s). MDPI and/or the editor(s) disclaim responsibility for any injury to people or property resulting from any ideas, methods, instructions or products referred to in the content.